

# Deep-time thermal history of the Great Unconformity in the Grand Canyon, USA: Combined zircon (U-Th)/He and K-feldspar <sup>40</sup>Ar/<sup>39</sup>Ar thermochronometers

# O.G. Thurston<sup>1,†</sup>, W.R. Guenthner<sup>2</sup>, K.E. Karlstrom<sup>3</sup>, M.T. Heizler<sup>4</sup>, J.W. Ricketts<sup>5</sup>, and K.T. McDannell<sup>6</sup>

- <sup>1</sup>Department of Earth and Environmental Sciences, Norwich University, Northfield, Vermont 05663, USA
- <sup>2</sup>Department of Earth Science and Environmental Change, University of Illinois at Urbana-Champaign, Urbana, Illinois 61801, USA
- <sup>3</sup>Department of Earth and Planetary Sciences, University of New Mexico, Albuquerque, New Mexico 87131, USA
- <sup>4</sup>New Mexico Bureau of Geology and Mineral Resources, New Mexico Tech, Socorro, New Mexico 87801, USA
- <sup>5</sup>Department of Earth, Environmental and Resource Sciences, University of Texas at El Paso, El Paso, Texas 79968, USA
- <sup>6</sup>Department of Earth Sciences, Dartmouth College, Hanover, New Hampshire 03755, USA

## **ABSTRACT**

Deep-time thermochronology by the zircon (U-Th)/He (ZHe) method is an emerging field of study with promise for constraining Precambrian rock thermal and exhumation histories. The Grand Canyon provides an opportunity to further explore this method because excellent geologic constraints can be integrated with multiple thermochronometers to address important questions about the spatial variability of basement erosion below the sub-Cambrian Great Unconformity composite erosional surface. In this study, we synthesize new ZHe results (n = 26) and published (n = 77) ZHe data with new Kfeldspar  $^{40}$ Ar/ $^{39}$ Ar data and models (n = 4) from Precambrian basement rocks of the Grand Canyon, USA. We use HeFTy and QTQt thermal history modeling to evaluate the ability of the individual ZHe and Kfeldspar 40Ar/39Ar thermochronometric data sets to resolve Precambrian thermal histories and compare those results with jointly modeled data using the QTQt software. We also compare Precambrian basement thermal histories of the eastern and western Grand Canvon, where the eastern Grand Canvon has  $\sim$ 4 km of Grand Canyon Supergroup strata deposited and preserved, and the western Grand Canyon, where the Supergroup was either never deposited or not preserved. In all locations, models constrained only by ZHe data have limited resolving power for

W.R. Guenthner https://orcid.org/0000-0003 -0895-3351 \*othursto@norwich.edu

GSA Bulletin; published online 6 May 2024

the past  $\sim$ 600 m.y., compared to models that combine K-feldspar 40Ar/39Ar and ZHe data, which extends the recorded history into the Mesoproterozoic. Our model results suggest that two regional basement unroofing events occurred. A ca. 1350-1250 Ma cooling event is interpreted to record basement exhumation from depths of  $\sim$ 10 km, and a second cooling episode ( $\sim$ 200–100 °C total) records exhumation from a depth of  $\sim$ 3 km to 7 km to near-surface conditions between ca. 600 Ma and 500 Ma. Easternmost Grand Canyon models suggest that the preserved maximum  $\sim$ 4 km thickness of the Grand Canyon Supergroup (with burial heating at  $\sim$ 100 °C) approximates the total original Mesoproterozoic and Neoproterozoic stratal thickness. Whether these Supergroup rocks were present and then eroded in the western Grand Canyon, as suggested by regional geologic studies, or were never deposited is not constrained by thermochronological data.

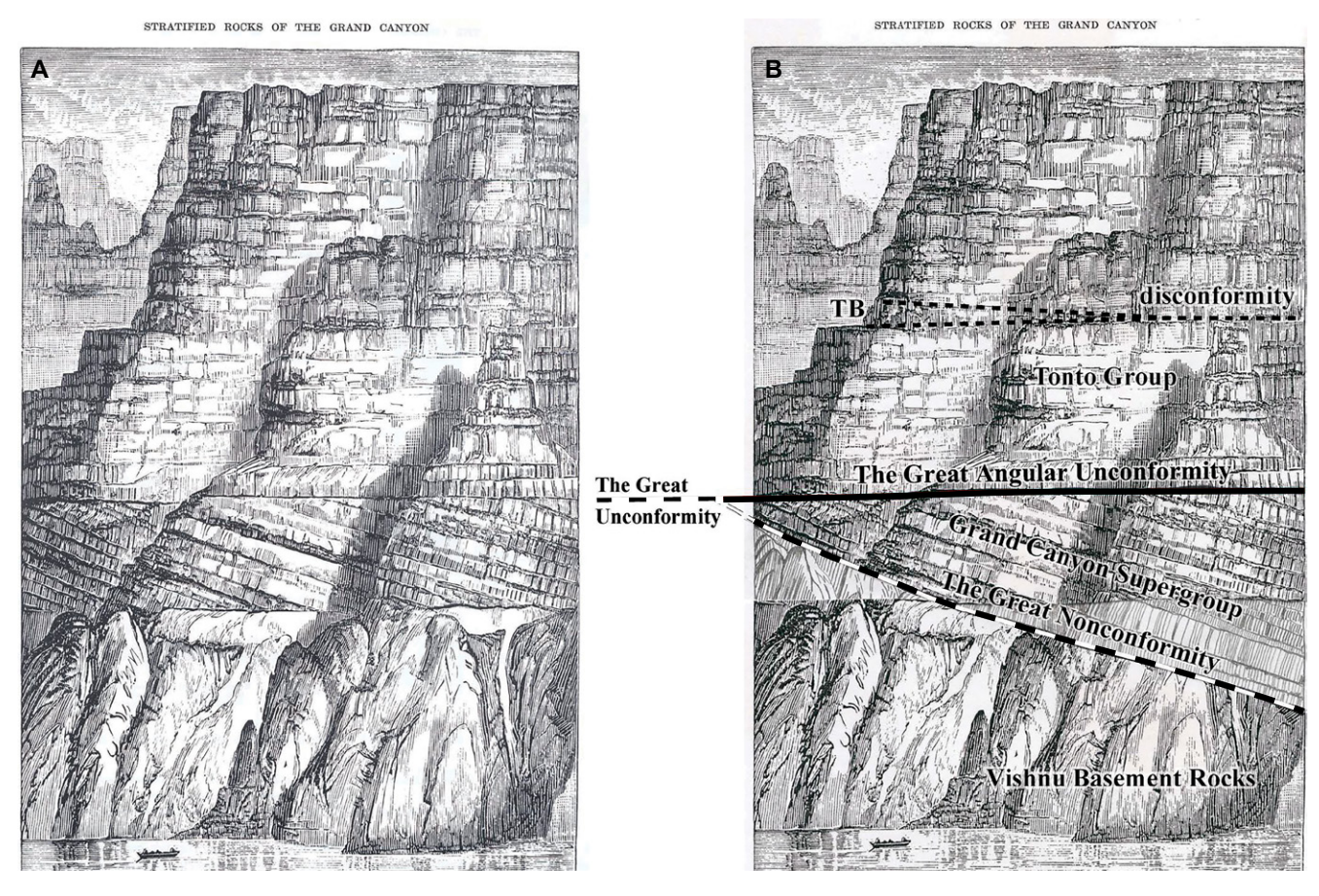
#### 1. INTRODUCTION

The zircon (U-Th)/He (ZHe) thermochronometer is a useful tool for exploring deep-time (before 1 Ga) thermal histories, particularly the ∼300–150 °C cooling histories of Precambrian crystalline basement rocks that unconformably underlie Phanerozoic sedimentary strata. Numerous recent papers have investigated the possible mechanisms responsible for the erosional history of this "Great Unconformity" (DeLucia et al., 2018; McDannell et al., 2018, 2022a; Keller et al., 2019; Flowers et al., 2020; Kaempfer et al., 2021; Peak et al., 2021; Ricketts et al., 2021; Thurston et al., 2022; McDannell

and Keller, 2022). The origins of this erosional surface (or surfaces) remain debated. Several non-mutually exclusive models have been proposed, which include  $\sim$ 3–5 km of globally averaged erosion driven primarily by continental glaciation during Snowball Earth (Keller et al., 2019; McDannell et al., 2022a; McDannell and Keller, 2022), dynamic uplift initiated by mantle plume impingement and underplating (McDannell et al., 2018) followed by lower crustal delamination (DeLucia et al., 2018), and broadly defined rift-related tectonism during the protracted breakup of supercontinent Rodinia (Flowers et al., 2020; Ricketts et al., 2021). The observation that many unconformities can merge into one composite Great Unconformity (Karlstrom and Timmons, 2012a) invites models incorporating multiple mechanisms and episodes of erosion.

The Grand Canyon, USA, is an important testbed for evaluating these hypotheses with potentially global implications. The Great Unconformity was first defined by Dutton (1882) after John Wesley Powell (1875) described two major unconformities in the eastern Grand Canyon, one below the Cambrian Tonto Group, and the other below the Mesoproterozoic Unkar Group (Fig. 1). These multiple unconformities offer a unique perspective on the composite nature and multiple episodes of erosion and deposition (Timmons et al., 2005; Karlstrom and Timmons, 2012a) that merge in many locations into what has been referred to as the Great Unconformity, where Cambrian sedimentary units directly overlie Precambrian crystalline basement (Fig. 1C). In the eastern Grand Canyon, the Mesoproterozoic and Neoproterozoic sedimentary basin strata provide constraints for

https://doi.org/10.1130/B37358.1.



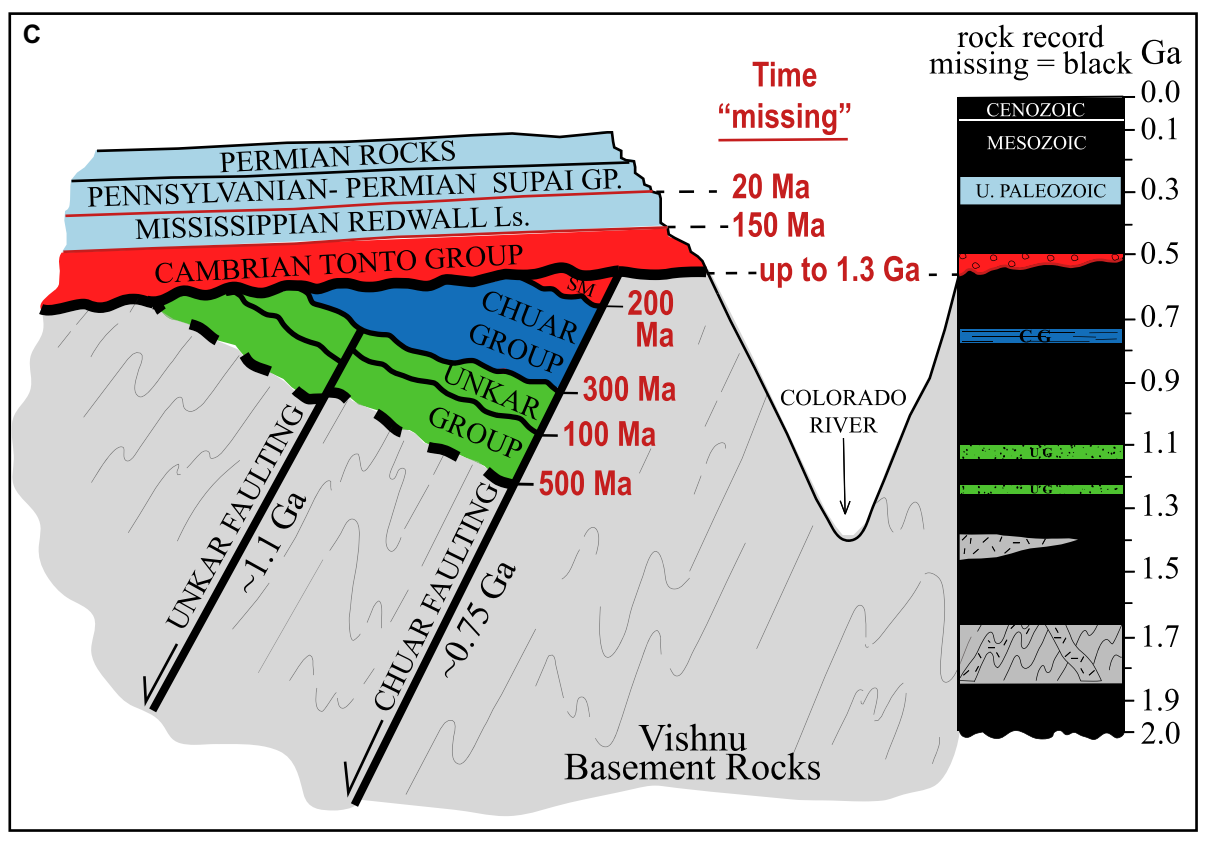


Figure 1. (A) John Wesley Powell (1876) recognized two major unconformities that bound three main sets of rocks: Vishnu basement rocks, Grand Canyon Supergroup, and Paleozoic strata. (B) Image shows the lower unconformity drawn correctly (from Karlstrom and Timmons, 2012a). (C) Grand Canyon has a relatively complete geologic record, yet more time is "missing" (black) than is recorded. Numeric ages for time "missing" (in red) are from Karlstrom et al. (2021). CG—Chuar Group; Gp.—Group; UG—Unkar Group; Ls—limestone; TB—Temple Butte; U—upper.

thermochronological models. These same rocks are absent in the western Grand Canyon. A key question is whether this absence is due to nondeposition (Peak et al., 2021) or a lack of preservation (Karlstrom et al., 2022).

This study has two goals. First, the modeling goal is to test the resolving power of the deep-time ZHe thermochronometer using all of the available ZHe data from prior papers,

Α

26 new ZHe dates reported here (Fig. 2), and joint modeling of ZHe with new K-feldspar <sup>40</sup>Ar/<sup>39</sup>Ar multi-diffusion domain (MDD) models and unequivocal (i.e., observed stratigraphic) geologic constraints. Generating and interpreting thermal histories derived from data sets that are under-constrained or models that are non-unique provides a challenge for reaching a consensus on the thermal history of both

Lees

the eastern and western Grand Canyon. We take special care in the design and interpretation of the model results presented here to provide the most plausible and appropriately complex thermal histories that are consistent with the combined data sets. The thermal history models explore not only what the data reveal about the thermal history of the Grand Canyon, but also modeling nuances such as the use (and misuse)

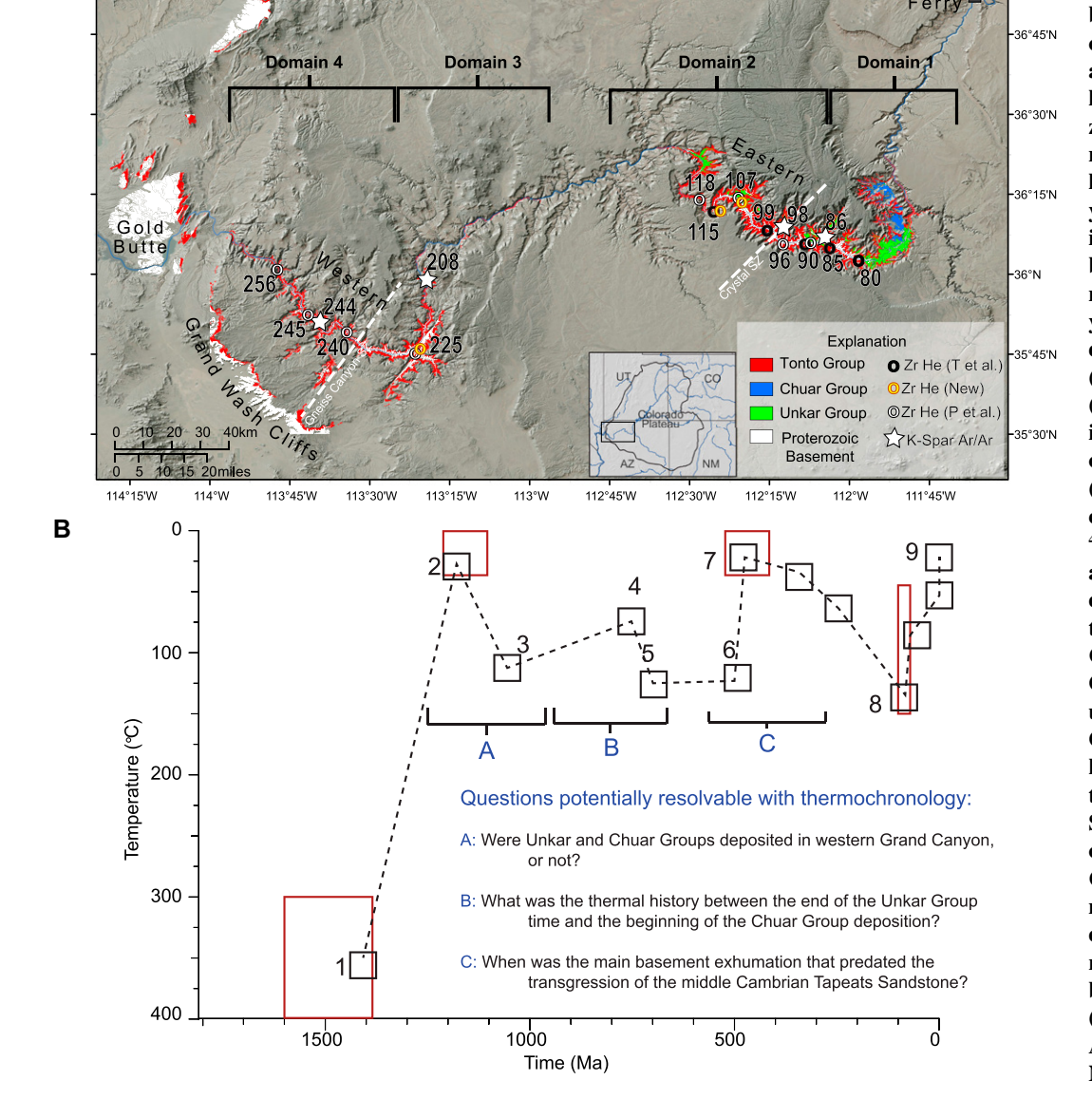


Figure 2. (A) Map of the Grand Canyon region, modified from Thurston et al. (2022). Symbols denote newly and previously reported ZHe (circles) and K-feldspar (stars) sample locations from Paleoproterozoic basement labeled by river mile. Eastern Grand Canyon locally preserves Grand Canvon Supergroup (Unkar Group in green; Chuar Group in blue) directly overlying basement; western Grand Canyon has Tonto Group (red) directly overlying basement. (B) Geologic constraint boxes (red) used for inverse modeling in HeFTy and QTQt and other geologic constraints (black boxes are not used as constraint boxes): (1) mica <sup>40</sup>Ar/<sup>39</sup>Ar basement cooling ages; (2) Unkar box used for eastern Grand Canyon and tested for western Grand Canyon; (3)  $\sim$ 2 km of Unkar Group deposition; (4) angular unconformity base of Chuar Group of a few degrees; (5)  $\sim$ 2 km of Chuar Group deposition atop the Unkar Group; (6) Sixtymile Formation deposited on Chuar Group; (7) Middle Cambrian to Devonian sedimentary strata deposited on exhumed basement; (8) Phanerozoic sedimentary burial before the Laramide orogeny; (9) multi-stage canyon carving. AZ-Arizona; CO-Colorado; NM-New Mexico, UT-Utah.

of constraint boxes in modeling. We compare alternative modeling approaches using HeFTy (ZHe only; Ketcham, 2005), QTQt (with ZHe alone and with combined ZHe and K-feldspar <sup>40</sup>Ar/<sup>39</sup>Ar MDD; Gallagher, 2012), and standalone K-feldspar <sup>40</sup>Ar/<sup>39</sup>Ar MDD (Lovera et al., 1989). The modeling goal explores how the ZHe-only models (i.e., the approach of Peak et al., 2021; Thurston et al., 2022) may be improved using multiple thermochronometers to achieve better resolution of time and temperature (e.g., McDannell et al., 2019; McDannell and Flowers, 2020).

The second goal, which is geological, is to seek the most probable thermal history for basement rocks in different segments of the Grand Canyon as they were cooled (and/or reheated) through the ~275–150 °C temperature window (~6–11 km depth for a 25 °C/km geothermal gradient) before being covered by the Cambrian Tonto Group. Specifically, we address the extent to which thermochronological data can resolve whether (Karlstrom et al., 2022) or not (Peak et al., 2021, 2022) Grand Canyon Supergroup strata could have been deposited in the western Grand Canyon.

# 2. TECTONIC AND THERMOCHRONOLOGICAL BACKGROUND

## 2.1. Grand Canyon Geology

The Grand Canyon has a relatively complete geologic record, yet more time is missing than recorded. Figure 1C summarizes the stratigraphic ages of rocks (from Karlstrom et al., 2021) that include: Paleoproterozoic crystalline basement rocks (1840-1370 Ma), Unkar Group (1250-1100 Ma), Chuar Group (775-729 Ma), Tonto Group (527–495 Ma), and other Paleozoic strata. The "time column" highlights the unconformities for which deep-time thermochronology may be able to help quantify the magnitude of basement cooling/exhumation prior to (1) the sub-Unkar Group unconformity (1370-1250 Ma); (2) the sub-Chuar Group slight angular unconformity (1100-775 Ma; Timmons et al., 2005); and (3) the sub-Tonto Group unconformity, which is variably expressed as the Tontoon-Chuar (729-500 Ma) and Tonto-on-Unkar (1100-500 Ma) angular unconformities, or the Tonto-on-basement unconformity (as old as 1840-500 Ma; Karlstrom et al., 2018, 2020, 2021). Figure 1C shows times of known basement heating due to sedimentary burial. The Unkar and Chuar groups of the Grand Canyon Supergroup are each  $\sim$ 2 km thick, with eroded tops, which indicates >100 °C of burial reheating for basement samples in the easternmost

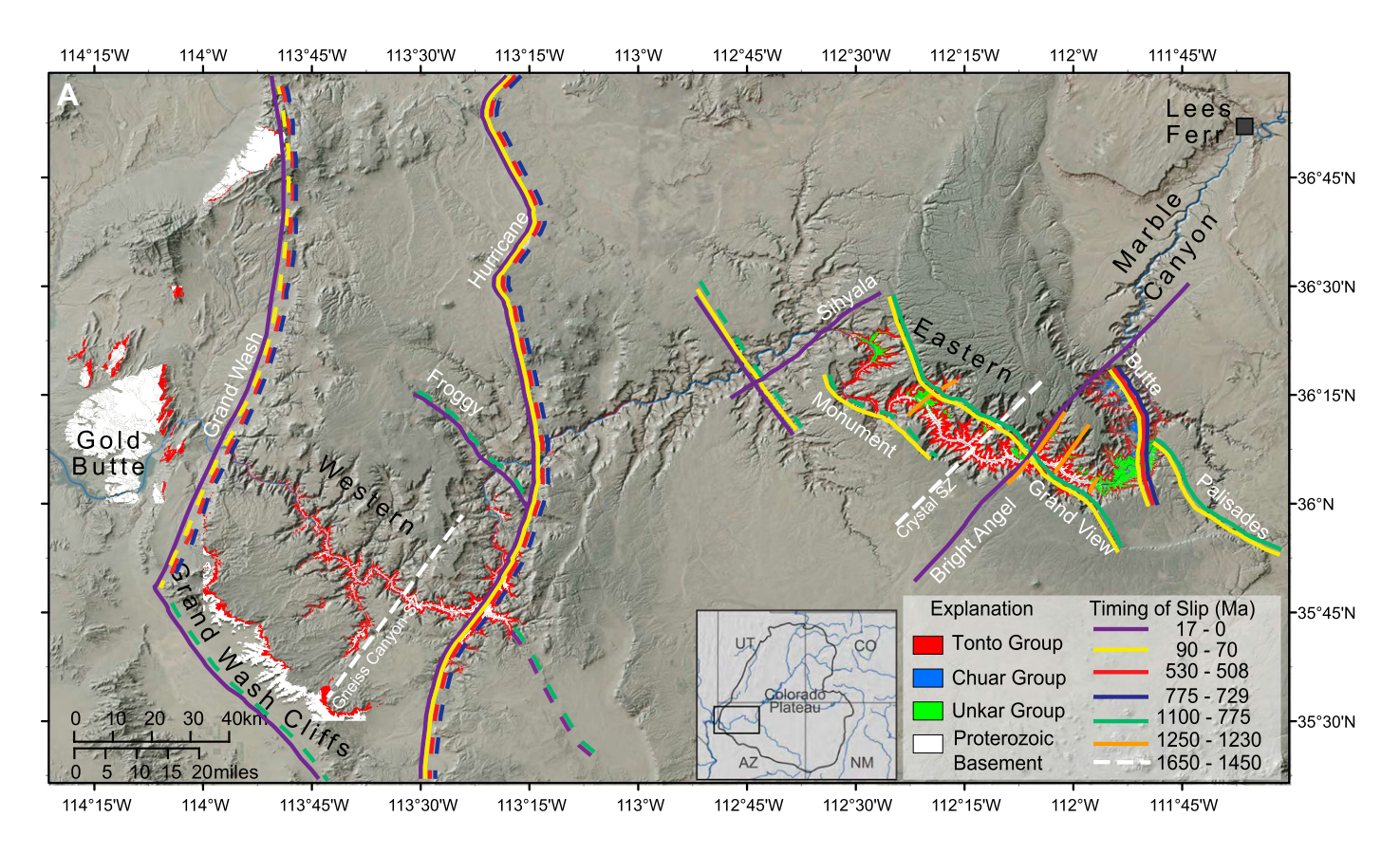
Grand Canyon, where the Chuar Group was deposited atop the Unkar Group (Fig. 2B).

Figure 3A shows the complexity of shear zones and fault systems that may have influenced differential basement cooling and exhumation. Dashed symbols show known and possibly younger reactivations of older fault systems (Karlstrom and Timmons, 2012b). Mesoproterozoic ductile shear zones (white lines in Fig. 3A) may separate blocks with different 1450-1250 Ma cooling histories based on <sup>40</sup>Ar/<sup>39</sup>Ar dating of biotite and K-feldspars (Karlstrom et al., 2003; McDermott, 2011). Northeast-striking, high-angle reverse faults (orange lines in Fig. 3A) had SE-up displacement on the scale of hundreds of meters synchronous with Unkar Group deposition (Timmons et al., 2005). Northwest-striking normal faults (green lines) have <1-2 km stratigraphic separation and segment the eastern Grand Canyon into half grabens that show movement at ca. 1100 Ma and do not offset the Chuar Group (Timmons et al., 2005). The W-down Butte normal fault (solid blue line) was active during Chuar deposition (775-729 Ma) to form and segment the Chuar basin (Timmons et al., 2001) and was inverted in the Cambrian (Karlstrom et al., 2018). Miocene normal faults (purple) increase in W-down slip toward the west; the Sinyala fault is a W-down normal fault that offsets upper Paleozoic strata with only a few meters of displacement and no known ancestry (Huntoon et al., 1996, but cf. Peak et al., 2021). Figure 3B provides a visual panorama of the combined Unkar-Chuar fault block in the eastern Grand Canyon. The Chuar Group rests with mild angular unconformity and in a contiguous stratigraphic section on the full preserved thickness ( $\sim$ 2 km) of the Unkar section in this fault block. Both groups are beveled by the sub-Tonto Group angular unconformity.

# 2.2. Prior ZHe Thermochronology

Studies by Peak et al. (2021) and Thurston et al. (2022) were the first attempts to apply the ZHe thermochronometer to understand basement exhumation histories in the Grand Canyon. These two studies interpreted and modeled clear trends among single-grain ZHe dates and effective uranium (eU =  $U + 0.238 \times Th$ ) concentrations, but in different parts of the canyon. For zircon crystals that have experienced the same thermal histories, differences in eU concentrations among crystals are proportional to differences in the degree of radiation damage, which in turn determines the He diffusivity and closure temperature of a given crystal (Guenthner et al., 2013). Multiple zircon grains from a single sample can therefore be used to investigate a range of closure temperatures, provided the sample (or group of samples) has a range of eU concentrations and displays a single date-eU trend. A model that parameterizes the damagediffusivity relationship in zircon, the zircon radiation damage and annealing model (ZRDAAM, Guenthner et al., 2013), can be used to reconstruct thermal histories from observed ZHe date-eU trends. Many rock samples, including those collected from the Grand Canyon basement rock, do not show a single, clear date-eU trend, but instead display a large amount of scatter (Peak et al., 2021; Thurston et al., 2022). If multiple samples are dispersed or potentially contain multiple trends, they may record different thermal histories and can be modeled as distinct groups, provided that there is a geologic explanation (e.g., discrete structural blocks) for the presence of multiple thermal histories in a region. Alternatively, data sets with large amounts of scatter can be attributed to uncertainties related to eU concentrations (Guenthner et al., 2016) and U and Th zonation (Hourigan et al., 2005), which together create single-grain date errors that exceed analytical uncertainties, even for samples with simple histories like laboratory age standards (e.g., Gleadow et al., 2015). That is, the damage-diffusivity relationship is not the sole source of date variation in a sample, and the ability of ZRDAAM to constrain thermal histories is confined mainly to those samples in which radiation damage is the dominant source of dating variation.

Thurston et al. (2022) focused on the eastern Grand Canyon, and Peak et al. (2021) focused on the western Grand Canyon, although both studies published data from both segments. The eastern Grand Canyon spans river mile 78-135 (river miles on the Colorado River are measured downstream from Lees Ferry, Arizona, USA). Here, the Grand Canyon Supergroup is preserved in most fault blocks; western Grand Canyon basement crops out from river mile 208 to river mile 260 and does not expose Grand Canyon Supergroup strata. Cambrian Tonto Group directly overlies the crystalline basement across both segments (Fig. 2A). These two studies agreed that (1) multiple unconformities or erosional surfaces (and related cooling trends in thermal history modeling) comprise the Great Unconformity in the Grand Canyon (Karlstrom and Timmons, 2012a); (2) there may have been different time-temperature (t-T) paths for samples collected across faults and shear zones that can be investigated by thermochronological data; and (3) the western and eastern Grand Canyon transects had different thermal histories, at least to the extent indicated by different Unkar/Chuar records of deposition or preservation. These basement reaches also had different Proterozoic cooling histories at 1680 Ma and post-1400 Ma



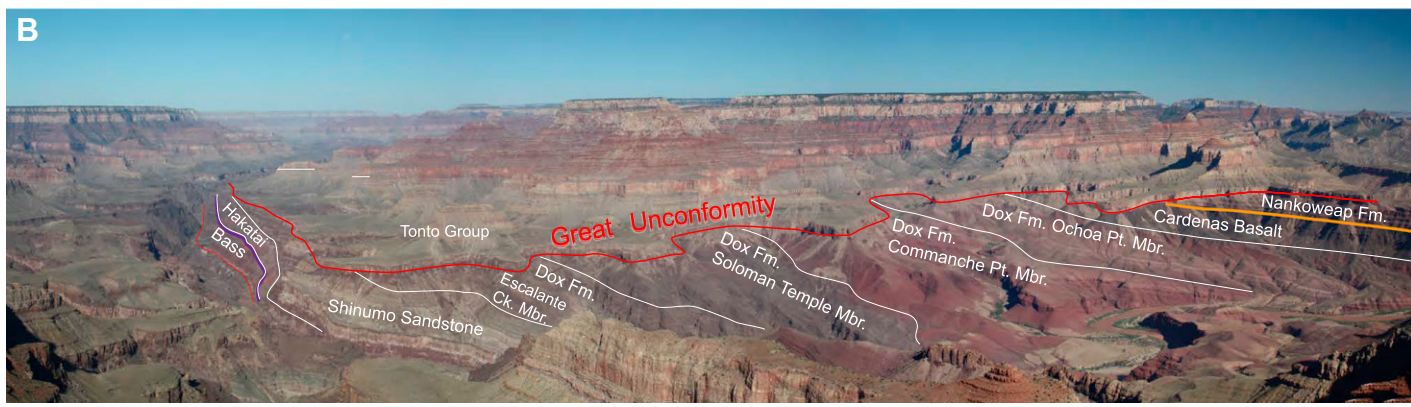


Figure 3. (A) Structural segmentation of basement rocks of the Grand Canyon region: white—ductile shear zones; orange—syn-Unkar SE-up reverse faults; green—1.1 Ga to 0.775 Ga (late to post-Unkar) NE-down normal faults; blue—0.775–0.73 Ga (syn-Chuar); red—W-down normal fault reactivated W-down faulting in the Cambrian (e.g., Butte fault); yellow—Laramide faults with possible Neoproterozoic—Cambrian ancestry; purple—Neogene normal faults. Arrow shows view of Figure 3B. (B) Panoramic view of multiple great unconformities (white arrow in 3A): sub-Unkar Group (Gp.) unconformity (purple line) records a major basement unroofing episode from ~10 km depth to the surface between 1350 Ma (mica \$^{40}\$Ar/\$^{39}\$Ar ages) and 1250 Ma. Normal faults tilted the Unkar Group and caused additional basement cooling in upthrown blocks at ca. 1.1 Ga. The sub-Chuar unconformity (orange line) is a very low-angle angular unconformity only preserved in the eastern Grand Canyon, which indicates limited additional basement exhumation between 1.1 Ga and 0.775 Ga. The post-506 Ma Tonto Group overlies tilted fault blocks of Unkar Group, Chuar Group, and Cambrian Sixtymile Formation (Fm.) with angular unconformity. Mbr.—Member.

(Karlstrom et al., 2003) and different Cenozoic cooling histories (Flowers et al., 2008; Flowers and Farley, 2012; Karlstrom et al., 2014), which makes them a good testbed for continued thermochronological studies.

Both studies used HeFTy modeling of composite ZHe data sets but arrived at different conclusions. Thurston et al. (2022) concluded that the ZHe data in the eastern Grand Canyon are consistent with the geologic data in recording

a dominant basement cooling event from 1300 Ma to 1250 Ma, prior to 1255 Ma deposition of the Unkar Group, but they argued that the present ZHe data are insensitive to the "ups and downs" of 1300–550 Ma fault-influenced basin

formation and basin-margin basement exhumation, which is well documented in the eastern Grand Canyon. Thurston et al. (2022) found very young ZHe dates (7–3 Ma), which suggests that the ZHe data and models were sensitive to a late Phanerozoic reheating/cooling event, including canyon carving (Karlstrom et al., 2014). Crucially, Thurston et al. (2022) showed that the reheating to temperatures within the ZHe partial retention zone during the most recent Cenozoic part of the Grand Canyon's thermal history can significantly overprint, and in some cases reset or obscure, the Neoproterozoic sensitivity of the ZHe thermochronometer. Peak et al. (2021) argued that their ZHe data were sufficiently sensitive to distinguish between thermal scenarios with and without the Grand Canyon Supergroup strata deposited in the western Grand Canyon, and they concluded that the western Grand Canyon may have been a basement paleo-high during the time of Grand Canyon Supergroup deposition in the eastern Grand Canyon, such that the Grand Canyon Supergroup was never present in the western Grand Canyon. The different conclusions reached by these two studies are the result of the two separate data sets each study examined and fundamental differences in modeling techniques and philosophy. In addition to samples from Mesoproterozoic basement, Thurston et al. (2022) presented a data set that included several 1.1 Ga diabase zircons, while Peak et al. (2021) reported Neoproterozoic dates from a 729 Ma ash at the top of the Chuar Group. Here, we restrict the discussion to basement samples, because the Supergroup samples in both studies are too limited to resolve their respective portions of overall basement cooling and should not be modeled with basement zircons. The contrasting views on modeling philosophy are explored in detail here by combining both data sets from Peak et al. (2021) and Thurston et al. (2022), along with new data from this study. Using this larger data set, we apply and evaluate a variety of modeling approaches involving the use of HeFTy and QTQt modeling software, MDD modeling combining ZHe with K-feldspar <sup>40</sup>Ar/<sup>39</sup>Ar, and applying both inverse and forward models. This expanded modeling approach employing multiple thermochronometers was useful for constraining the t-T paths that best predict the observed data.

### 3. METHODS

# 3.1. Zircon (U-Th)/He Methods

New analyses of 26 single-grain ZHe dates (Table 1) were conducted at the University of Illinois at Urbana-Champaign following methods described in Guenthner et al. (2016).

Helium measurements were collected under vacuum with a Pfeiffer PrismaPlus OMG-220 spectrometer, while U and Th were collected on a ThermoScientific iCAP Q inductively coupled plasma-mass spectrometer. Alphaejection corrections followed the equations and methods of Hourigan et al. (2005). A limitation of the data set we compiled is that zircon samples were collected over several decades for different initial project goals. Ideally, ZHe dates and K-feldspar 40Ar/39Ar spectra would have been collected from the same rock. Thus, we cannot rule out complexities that could be due to different rock types (e.g., differences in mineral zoning) and cooling histories among the sampling locations, which may be separated by underappreciated faults and shear zones. These potential complexities are of particular concern for metamorphic samples that could retain thermal histories of their protolithic material. Analyses from the different labs reflect slightly different sample locations (Fig. 4), and a focus on metamict grains, which yielded young Cenozoic ages in Thurston et al. (2022), but not in Peak et al. (2021). Modeling specifics are provided in Tables S1 and S3 in the Supplemental Material1.

## 3.2. 40Ar/39Ar Methods

K-feldspar thermochronological modeling is based on the MDD method of Lovera et al. (1989); details of data collection closely follow those described in Sanders et al. (2006). Argon geochronological data for this study are provided in the Supplemental Material. All K-feldspars were step-heated in a double vacuum resistance furnace using between 34 and 46 heating steps, and isotopes were measured on either a MAP 215-50 single-collector mass spectrometer or a ThermoScientific Helix multicollector (MC) mass spectrometer. K-feldspar age spectra for samples T02-86-2 and T0-98-14 were presented in Timmons et al. (2005), as were MDD results for T0-98-14. Data from sample T0-98-14 are presented again in full here for incorporation into the OTOt combined models. New MDD modeling was done for sample T02-86-2, whereas data for samples H21-208.3a and MH10-244.8 are new.

## 3.3. Modeling Methods and Strategies

Continued challenges specific to the ZHe method include a better understanding of annealing kinetics of radiation damage (Guenthner, 2021) and how damage influences He diffusion kinetics, and thus temperature sensitivity, within single grains and parts of zoned zircon grains (Hourigan et al., 2005; Ginster et al., 2019). A broader set of challenges involves the optimal approaches to resolving thermal histories from data sets that are inherently under-constrained and non-unique. The choice of modeling methods for constraining deep-time thermochronology is therefore an important consideration for assessing both the plausibility of a particular t-Tscenario, but also the degree to which the complexity of a t-T path is revealed by the data, or merely a product of a priori constraints. To assess t-T path complexity through this lens, the modeling goals for this study were to (1) combine ZHe and 40Ar/39Ar data to generate a more robust thermal history for four shear zone-bounded segments of the Grand Canyon (Fig. 5), (2) allow the models to be predominantly driven by data rather than external constraints, (3) use geologically indisputable constraints, and (4) test the sensitivity of different data sets to various time periods in the thermal history of the Grand Canyon. In pursuit of these goals, we explore the differences among thermal history models derived solely from ZHe data (using HeFTy and QTQt), solely from K-feldspar 40Ar/39Ar MDD modeling (after Lovera et al., 1989), and from jointly modeled ZHe and K-feldspar 40Ar/39Ar data (using QTQt). Tables S2, S4, and S5 provide raw <sup>40</sup>Ar/<sup>39</sup>Ar data and data processing information.

# 3.3.1. QTQt Thermal History Modeling

To best address the first two modeling goals, we used QTQt (Gallagher, 2012) as our main modeling software. QTQt allows all of the available data (both ZHe and 40Ar/39Ar) for each subregion of the Grand Canyon to be input and modeled simultaneously. The kinetics for each system included the MDD model for K-feldspar <sup>40</sup>Ar/<sup>39</sup>Ar (Lovera et al., 1989) and the zircon radiation damage and annealing model (ZRDAAM) for ZHe (Guenthner et al., 2013). QTQt also allows for data uncertainty resampling, which is an important consideration for ZHe data sets because multiple sources of uncertainty in ZHe data need to be considered and explored during modeling, including those related to eU concentrations (Guenthner et al., 2016) and U and Th zonation. Forward models of date-eU correlations show that the range of dispersion observed in most ZHe data sets cannot be explained with our current understanding of the damage-diffusivity relationship alone

<sup>&</sup>lt;sup>1</sup>Supplemental Material. Additional modeling methodology and results, including comparisons of measured versus modeled (U-Th)/He zircon ages modeled in both QTQt and HeFTy, detailed Ar/Ar MDD modeling methods, Domain 2 QTQt models, and an assessment of grain selection for HeFTy models. Please visit https://doi.org/10.1130/GSAB .S.25488559 to access the supplemental material; editing@geosociety.org with any questions.

						1		, ,		J			,					
	Corr. date analytic unc. (Ma)		31	0 6 9 5 5 5 6 6 6 6 6 6 6 6 6 6 6 6 6 6 6	9	∠£000000 80000	4 0 0 1 1 2 2	t	72	17 27 58 58 14	80	∞∞4≈≈∞ <del>0</del>		12	71 14 14 15 15 15 15 16 16 17 17 18 18 18 18 18 18 18 18 18 18 18 18 18	84 & L O 4	-21~0	(Continued)
	Corr. Date (Ma)		447	132 560 96.3 167 168	206	337 470 255 74.5 223 212	69.0 249 74.7 176	2	682	522 740 594 578 501 267	582	639 454 228 228 246 506 746		512	699 364 710 631 401 469	201 165 142 232 252 376	136 223 334 377	ی
	FT comb		0.64	0.73 0.56 0.72 0.58 0.65	0.59	0.68 0.68 0.58 0.58 0.65 0.72	0.63 0.67 0.73 0.64	7.0	0.77	0.69 0.80 0.77 0.80 0.81	0.65	0.80 0.83 0.68 0.72 0.72		0.63	0.71 0.66 0.74 0.73 0.73	0.60 0.64 0.59 0.67 0.65	0.73 0.62 0.69 0.73	
	Uncorr. date analytic unc. (Ma)		9	7. 6.0 9.1 9.1	7	44 ω ∟ ω α α	£. 80.4 £	2	2	o 5225 o	2	<b>≻</b> ₩₩₩₩₩		4	ი <u>ან</u> 44 ოთ	∞ ∞ ∞ ∞	1581	
	Uncorr. Date (Ma)		292	96.2 319 69.1 97.4 110.3	122	231 324 149 43.2 153	43.2 169 54.5 114	<del>-</del> 3	534	364 602 445 452 217	376	514 376 237 155 201 365 586		328	503 243 537 415 297 390	122 106 84.2 157 200 247	136 137 230 277	
	eU		629	371 531 990 1305 851	202	1129 620 1059 936 1279 1033	1620 1283 1957 1123	2	365	522 169 437 384 325 809	360	232 232 583 589 358 215 170		991	587 943 542 486 922 819 658	509 529 608 258 372 211	329 351 381 448	
	#1		*	* * * * *	*	* * * * * *	* * * * *		*	* * * * *	0.003	0.004 0.007 0.005 0.005 0.004 0.004		*	* * * * * *	* * * * * *	0.004 0.090 0.058 0.15	
	Th (ng)		*	* * * * *	*	* * * * * *	* * * * *		*	* * * * *	0.206	0.320 0.545 1.39 0.426 0.754 0.289		*	* * * * * *	* * * * *	0.294 0.192 0.327 0.45	
	#		*	* * * * *	*	* * * * * *	* * * * *		*	* * * * * *	0.008	0.01 0.03 0.05 0.04 0.012		*	* * * * * *	* * * * *	0.010 0.004 0.008 0.01	
_	(gu)		*	* * * * *	*	* * * * * *	* * * * *		*	* * * * * *	0.665	1.07 2.61 4.14 1.27 3.61 0.994 0.848		*	* * * * * *	* * * * * *	0.929 0.335 0.753 1.42	
e DAT/	#		4	ε9- <u>4</u> /	ဗ	203007	464±α	0	-	იინთიი	-	0000		7	014104400	<b>0</b> 04+00	76 38 38	
U-Th)/H	Th (ppm)		169	190 183 133 275 240	77	1135 97 102 1040 226 213	511 362 204 257	5	101	130 170 99 99 191	104	182 182 183 183 183 183 183 183 183 183 183 183		219	131 214 129 245 245 183	<u>554</u> 688 88	267 284 308 363	
ZHe (	#		54	90425	7	01 8 12 25 13 13 13 13 13 13 13 13 13 13 13 13 13	27 33 37 37	9	ო	28839	ო	-100000-		Ħ	√400€04	± > 044 >	<b>ω</b> ωω4	
1. SUMMARY ZHe (U-Th)/He DATA	(mdd)		639	326 487 958 1239 794	487	860 597 1035 688 1225 982	1498 1197 1908 1062	2	341	492 155 411 361 764	336	131 221 540 546 341 201 159		939	556 892 502 455 865 761	468 500 574 237 346 191	267 284 308 363	
1. SU	#		S	-4-0-	-	ωω4-44	00000	)	ო	თ N 4	4	0000000		6	00V4044		− w 4 4	
TABLE	<sup>4</sup> He (nmol/g)		1097	194 939 371 690 511	336	1431 1115 864 218 1014 861	378 1185 577 696	63	1104	1060 579 1089 974 730 965	649	332 377 554 394 326 386 400		1802	1665 1262 1645 1127 1515 954 1434	337 222 222 407 288	213 242 429 597	
	Rs (μm)		35	843 83 83 83	28	37 27 28 28 33 41	38489 1388 1388 1388	4	52	37 60 52 52 62 62	32	54 54 54 54 54 54		31	04848448 0498488	3008878	44 30 37 45	
	Sample name and aliquot		CP06_70_bp_z01	CP06_70_bp_202 CP06_70_bp_203 CP06_70_bp_204 CP06_70_bp_205 CP06_70_bp_205	CP06-72_bp_z01	CP06-72_bp_z02 CP06-72_bp_z03 CP06-72_bp_z04 CP06-72_bp_z05 CP06-72_bp_z06 CP06-72_bp_z06	CP06-69_bp_z01 CP06-69_bp_z02 CP06-69_bp_z03 CP06-69_bp_z03	001	CP06-65_bp_z01	CP06-65_bp_202 CP06-65_bp_203 CP06-65_bp_204 CP06-65_bp_205 CP06-65_bp_205 CP06-65_bp_205	OT21-RM-224-1	OT21-RM-224-3 OT21-RM-224-4 OT21-RM-224-5 OT21-RM-224-7 OT21-RM-224-10 OT21-RM-224-10		UG90-2_bp_z01	UG90-2 bp 202 UG90-2 bp 203 UG90-2 bp 204 UG90-2 bp 205 UG90-2 bp 205 UG90-2 bp 207 UG90-2 bp 207 UG90-2 bp 207	UG96-1_bp_201 UG96-1_bp_202 UG96-1_bp_203 UG96-1_bp_204 UG96-1_bp_205 UG96-1_bp_205	K12-79.6-AW-1 K12-79.6-AW-3 K12-79.6-AW-6 K12-79.6-AW-8	
	Longitude (°W)		113.709		113.714		113.571		113.361		113.351			112.137		112.225	111.969	
	River Latitude mile (°N)		35.8788		35.9303		35.823		35.7736		35.7813			36.1015		36.1072	36.0504	
	River L mile		245 (		256 (		240		225		224 (			06		96	08	
		Western Grand Canyon West of Gneiss Canyon shear zone		<b>.</b>	Meriwhitica Monocline	o constant	Separation Batholith <sup>A</sup>	East of Gneiss Canyon	Diamond Creek Pluton granite <sup>A</sup>		Diamond Creek Pluton	ת מ	Eastern Grand Canyon East of Crystal shear	Horn Pluton	910000	96-Mile Pluton <sup>A</sup>	Rama schist <sup>в</sup>	

							TAE	TABLE 1. (Continued)	ontinue	g											
	River	River Latitude mile (°N)	Longitude (°W)	Sample name and aliquot	Rs (µm)	<sup>4</sup> He (nmol/g)	#	(mdd)	<b>a</b> )	Th (ppm)	H	n (Bu)	#	Th (ng)	Н	n ne	Uncorr. U Date a (Ma)	Uncorr. date analytic unc. (Ma)	comb	i	Corr. date analytic unc. (Ma)
				K12-79.6-AW-9 K12-79.6-AW-11 K12-796-AW-12	51 54 54	52.1 212 270	4.0.1	126 341 283	იოო	126 341 283	81 − 4 0 − 1	0.780 0. 1.10 0. 1.96 0.	0.010 0.01 0.02 0.02	0.195 0.338 0.231	0.114 0.004 0.030	156 421 350	71.9 107 169	2.6	0.76 0.71 0.78	94.4 150 218	2 - 3
Zoroaster Pluton	82	36.0892	112.06	K12-85.3L-AW_1	42	16.2	0.2	1252	12	129	15 3.9	3.95 0.	0.04 0.	4	0.05	1283	2.35	0.03	0.71	3.28	0.05
granodione				K12-85.3L-AW_4 K12-85.3L-AW_6 K12-85.3L-AW_7 K12-85.3L-AW_8 K12-85.3L-AW_12	44 43 10 10 10 10 10 10 10 10 10 10 10 10 10	23.6 23.6 23.1 11.8	0.000 1.452 1.000	630 537 636 706 573	00000	57 68 75 56	711 06 1.4.0.4	2.95 1.76 0.99 0.90 0.90 0.00	0.03 0.02 0.04 0.09 1	0.27 0.27 0.45 0.45 0.48	0.03 0.03 0.08 0.08	643 556 652 724 586	3.40 17.8 7.09 5.91 3.75	0.04 0.02 0.07 0.05	0.75 0.72 0.77 0.83 0.79	4.53 24.8 9.20 7.16 4.74	0.06 0.3 0.08 0.06
Horn Pluton	06	36.102	112.137	K12-90.4R-3	69	45.4	0.3	1283 12	1283	159 1	159 12.1		0.1	1.49 0	0.45 1	320	6.38	0.08	0.79	8.06	0.10
(a)				K12-90.4R-4 K12-90.4R-5 K12-90.4R-6 K12-90.4R-7	73 46 68 43	50.4 57.8 33.2 128	0.00 0.4 1.2 1.4	21135 12 2113 2: 1444 14	1235 2113 1444 1404	33 76 140 115	33 23.6 76 12.0 140 20.9 115 6.87		0.02 0.05 0.05 0.09	627 431 03 561	0.140 1 0.078 2 0.52 1 0.177 1	1243 2131 1477 1431	7.52 5.04 4.17 16.5	0.07 0.05 0.05 0.2	0.83 0.74 0.82 0.72	9.07 6.81 5.10 22.9	0.09 0.07 0.06 0.2
West of Crystal shear																					
Ruby Pluton granite <sup>A</sup>	107	36.2326	112.34	CP06-52 bp. 201 CP06-52 bp. 202 CP06-52 bp. 203 CP06-52 bp. 204 CP06-52 bp. 204 CP06-52 bp. 206 CP06-52 bp. 208 CP06-52 bp. 208 CP06-52 bp. 208 CP06-52 bp. 208 CP06-52 bp. 209 CP06-52 bp. 209 CP06-52 bp. 209 CP06-52 bp. 209 CP06-52 bp. 209 CP06-52 bp. 209 CP06-52 bp. 209	0480888888444 080888888444	1159 1603 424 3534 2049 1739 1510 1559 765 919 872	იით <u>ნ</u> ∠440ღლი	341 424 678 678 529 706 627 231 280	0 & 0 & 0 & 0 & - 1 × 4 4 4	3302 3357 6616 603 2297 2344 1882 212	იიი <u>ი</u> ი044000	* * * * * * * * * *	* * * * * * * * * *	* * * * * * * * * *	* * * * * * * * * *	413 466 666 666 666 709 709 709 709 709 709 709 709 709 709	500 558 94.9 43.1 54.9 355 394 497 535 545	124.08v04888	0.70 0.67 0.66 0.66 0.78 0.79 0.73 0.73	698 817 214 637 809 649 649 507 654 723	£54£8884±82£
Ruby Pluton granite <sup>c</sup>	107	36.2267	112.337	OT21-RM-107-1 OT21-RM-107-3 OT21-RM-107-3 OT21-RM-107-6 OT21-RM-107-6 OT21-RM-107-7 OT21-RM-107-1 OT21-RM-107-1		131 670 690 690 495 485 49.0 768 828 828 660 339	0,000-00000- 4 0	2224 2354 2352 244 244 244 244 244 244 244 244 244 2	-www-www	50 2205 2205 1126 105 1171 149		0.544 0.0937 0.0937 0.0336 0.110 0.110 0.310 0.310 0.310 0.310 0.310 0.310 0.310 0.310 0.310 0.310 0.310 0.310	0.006 0.001 0.001 0.001 0.001 0.004 0.003 0.002 0.001 0.001 0.001	0.307 1.13 0.425 0.505 0.41 0.0436 0.190 0.782 0.742 0.550	0.004 0.01 0.005 0.006 0.01 0.0015 0.003 0.009		286 216 371 371 304 304 402 260	ω0/4r044±ωr0ω	0.78 0.657 0.065 0.77 0.77 0.77 0.77	366 323 570 603 478 418 1325 394 352	4 ω ο <b>/</b>
Tuna Pluton granodiorite <sup>B</sup>	66	36.1444	112.255	K12-99R2-1	43	64.1	9.0	218	-	140	24 0.8			0.552 0	0.095	251	65.8	1.6	0.72	65.8	1.6
				K12-99R2-2 K12-99R2-4 K12-99R2-5 K12-99R2-6 K12-99R2-6	39 45 39 39 39	116 272 261 87.5 742	3.5	345 439 114 533	ωω4	307 314 125 21 257	288 28 28 28. 20 00.	0.700 0. 2.42 0. 0.756 0. 0.475 0.	0.005 0.02 0.005 0.003 0.01	0.623 1.73 0.502 0.086 0.578	0.086 0.15 0.111 0.038 0.071	218 218 119 593	78.8 130 298 186 327	<u>,</u> 40 4 70	0.65 0.75 0.73 0.72	78.8 130 298 186 327	6.0047
Elves Chasm granodiorite <sup>B</sup>	115	36.2037	112.426	K12-115L-3 K12-115L-4 K12-115L-5 K12-115L-8	47 60 49 49	134 91.1 102 162	1 0.6	532 229 329 668	യ നവന	166 75 111 132	2 10.1 2 2.6 5 4.5 5 4.5	0 m <b>-</b>	0.04 0.03 0.07	3.16 0.888 0.0.615 0.888	0.05 0.013 0.009 0.013	571 246 355 699	43.3 68.2 52.9 42.8	0.7 0.8 0.6		52.0 85.8 70.5 56.9	0.8 1.3 0.9
Elves Chasm granodiorite <sup>c</sup>	15	36.24	112.473	OT21-RM-120-1	31	554	8	417		207	2 0.0					.,	569	က	0.63	427	S
				OT21-RM120-2 OT21-RM120-3 OT21-RM120-4 OT21-RM120-7 OT21-RM120-8 OT21-RM120-9 OT21-RM120-9	40888489 40488609	239 313 301 212 384 171		318 326 404 384 508 336 124		158 234 202 162 118	0000-00 N-N	0.947 0.0816 0.0339 0.0732 0.0508 0.0608 0.06010 0.0601 0.0601 0.0601 0.0601 0.0601 0.0601 0.0601 0.0601 0.06010 0.0601 0.0601 0.0601 0.0601 0.0601 0.0601 0.0601 0.0601 0.0601 0.0601 0.0601 0.0601 0.0601 0.0601 0.0601 0.0601 0.0601 0.0601 0	0.011 0.010 0.004 0.009 0.001 0.007 0.007	0.471 0 0.362 0 0.196 0 0.103 0 0.404 0 0.575 0	0.006 0.004 0.003 0.005 0.005	185 334 272 148 185 357	148 300 217 135 170 329	ี ผพ ผ ผ ผ พ ผ <del>4</del>	0.73 0.66 0.69 0.73 0.70	203 394 330 195 410 410	04404ωn
Note: Uncorr.—uncorrected; unc.—uncertainty; Corr APeak et al. (2021). BThurston et al. (2022). CNew data. *Data unavailable.	ected; u ).	nc.—unce	rtainty; Corr	.—corrected.																	

Geological Society of America Bulletin

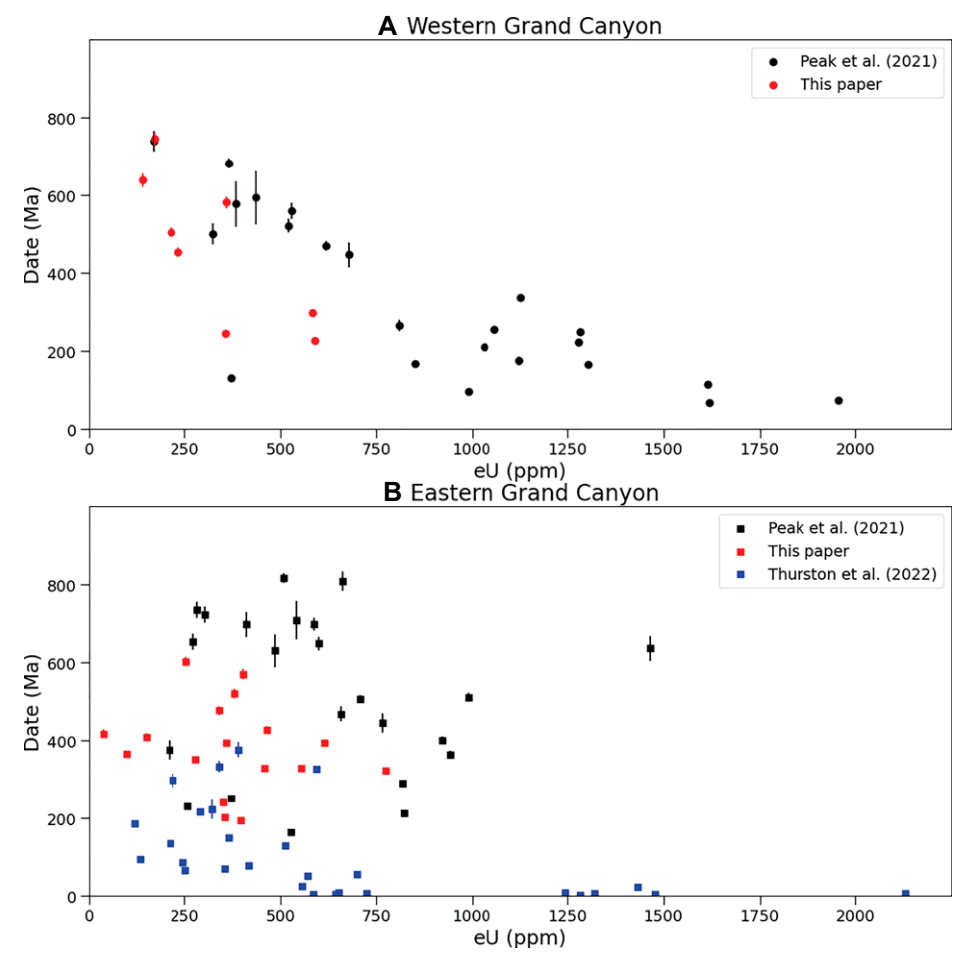


Figure 4. All available ZHe data from basement rocks of the Grand Canyon compiled from Peak et al. (2021, black), Thurston et al. (2022, blue), and new data from this study (red). Eastern Grand Canyon samples are squares; western Grand Canyon samples are dots. Large dispersion presents modeling challenges. Note post-6 Ma ages with a full range of eU (600–1500 ppm) that record rapid Cenozoic canyon carving.

(Guenthner, 2021). Zonation may be a plausible explanation for much of this excess dispersion (Guenthner et al., 2013), but methods for capturing U and Th zonation, crucially in full three-dimensional space, are not routinely implemented.

QTQt allows for these uncertainties to be explored using Bayes' hierarchical resampling of the unknown total date uncertainties (Gallagher, 2012). The uncertainties are randomly sampled from a normal distribution of the measurement error (scaled between minimum and maximum absolute value multipliers, i.e.,  $1-100\times$  the input errors). At a minimum, the hierarchical error resampling approach enables the data to directly guide uncertainty inference and the relative probability of a specific path. In our QTQt models, we used an input uncertainty for QTQt of 10% of the uncorrected ZHe date that was resampled during each reversible jump

Markov Chain Monte Carlo (rj-MCMC) run. QTQt models were run with 500,000 burn-in paths (used to fully explore t-T space and then discarded) initially and 500,000 retained postburn-in paths to estimate the posterior distribution. We accepted more complex models for equivalent likelihood to fully explore the entire t-T space and to retain the full complexity of the posterior distribution of t-T paths.

QTQt models also include geologic data, such as the ages of observed stratigraphic units, which are represented by a minimum number of geologic constraint boxes. Constraint boxes are shown in Figure 2B and further discussed below. Several groups of models were run without constraint boxes (Fig. 6) to assess which parts of *t-T* space the thermochronological data exhibited sensitivity, and to provide a baseline for comparison of models with and without constraint boxes to better understand how each constraint

impacts the thermal history. For our modeling goal, this comparison helps to determine the extent to which modeling outcomes are driven primarily by the ZHe data, the <sup>40</sup>Ar/<sup>39</sup>Ar data, the combined thermochronological data, undisputed geologic constraints, and hypothetical geological scenarios. For the geologic goal (Goal 2), such information is crucial in parsing the more probable thermal histories.

# 3.3.2. HeFTy Thermal History Modeling

Although we find the multi-thermochronometer QTQt output most compelling, we also show model results using the HeFTy thermal history modeling software (Ketcham, 2005). HeFTy output provides a useful comparison to previous Grand Canyon studies that relied either partially (Thurston et al., 2022) or solely (Peak et al., 2021) on HeFTy. One limitation of HeFTy is that it cannot model Ar diffusion in K-feldspar by the MDD method. As such, our HeFTy models only use ZHe data as thermochronometric inputs. A second limitation is that HeFTy cannot handle the large ZHe data sets required for proper deep-time t-T resolution, since the number of possible inputs that can be used in a single HeFTy model is limited to seven individual grains. Furthermore, an assumption in HeFTy is that the data uncertainty estimates are accurate. This assumption is invalidated since a well-known and persistent problem with zircon (U-Th)/He data is accounting for the total error related to individual dates (e.g., Flowers et al., 2023). One ad hoc approach to overcoming these issues consists of binning large, single-grain data sets by their eU concentrations and then averaging the dates of all grains that fall within a given bin such that the mean is a synthetic date, and the standard deviation is the error (Flowers and Kelley, 2011). An alternative, which we use here, is to select measured singlegrain dates that are representative of the overall observed date-eU trend. We acknowledge that this approach is different from the binning and averaging technique used in Peak et al. (2021) and Thurston et al. (2022), but arguably no less subjective; both require the user to preferentially pick a subset rather than use the entire data set (as in QTQt). Regardless of approach (synthetic grains versus a subset of measured grains), the trajectory of the ZHe date-eU trends is similar (Figs. S11-S13). We emphasize that the use of either grain subsets or synthetic grains results in either nearly identical inputs to HeFTy, or, in the case of Domain 4, the use of grain subsets provides a better approximation of the overall date-eU trend (Fig. S13). To address uncertainty in the data, HeFTy ZHe inputs used errors that were 10%-20% of the corrected ZHe date (Table 1; Table S3).

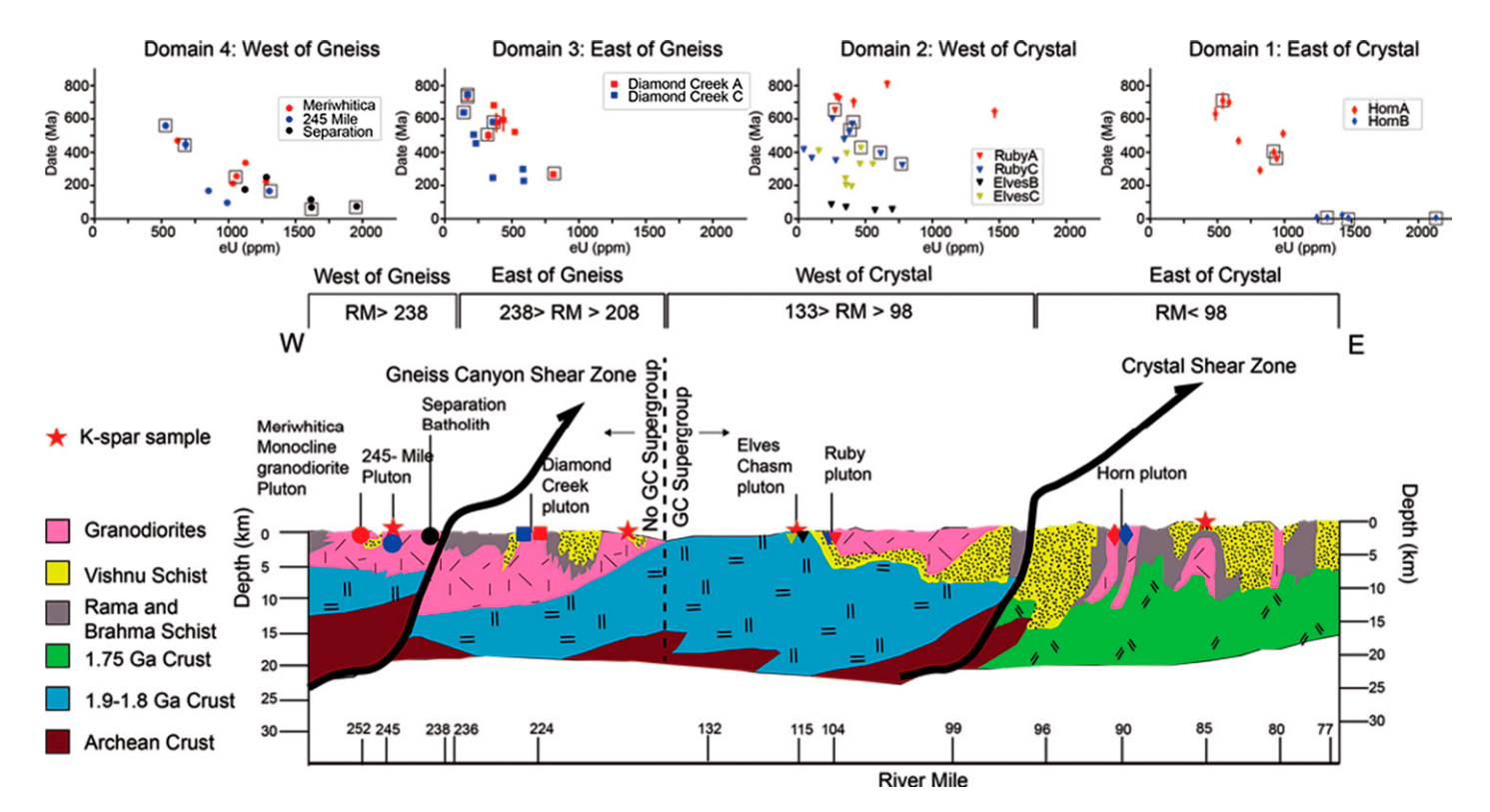


Figure 5. Cross section of basement units and major shear zones, modified from Holland et al. (2015). ZHe data from the Grand Canyon (GC) are divided by river mile (RM) according to the locations of sample sites relative to the Crystal shear zone at RM 98 and the Gneiss Canyon shear zone (RM 238). Eastern Grand Canyon has Grand Canyon Supergroup strata; western Grand Canyon preserves no Supergroup strata. Division of the ZHe data into domains helps reduce dispersion and generates somewhat clearer negative date-eU trends with the exception of data from west of the Crystal shear zone. Plots above each segment represent the ZHe inputs for our QTQt and HeFTy models. Red stars indicate locations of the K-feldspar samples used in the thermal history models.

# 3.3.3. Thermal History Geologic Constraints

Constraint boxes are used in both QTQt and HeFTy to represent prior information gleaned from geologic data (i.e., crystallization or stratigraphic age constraints). In cases where these geologic data are unequivocal, constraint box usage is relatively straightforward and an important component of thermal history modeling. However, an overabundance of constraint boxes can often mask the true resolving power of the thermochronological data because the outcome of the modeling is predetermined by constraintbox placement (i.e., the posterior simply becomes the prior). Each t-T box should therefore serve as either a constraint that is tied to an undisputed geologic event or as a means to heuristically test a scenario pertaining to the timing and temperature of a specific geologic phenomenon (e.g., McDannell et al., 2022a, 2022b, 2022c). In areas where geologic constraints are scarce, such as for the Precambrian in the western Grand Canyon, some t-T boxes are used strictly for such heuristic testing. Here, we distinguish these testing boxes from geologic constraint boxes.

To recover the most likely thermal history models for a given canyon segment or indi-

vidual sample, we ran models with what we consider to be undisputed geologic constraint boxes (the same boxes are used in both HeFTy and QTQt; Tables S1 and S3). The first three of the four total constraint boxes were applicable to the entire Grand Canyon region: (1) 300-400 °C, 1650-1450 Ma: cooling following peak metamorphic conditions as constrained by muscovite and biotite 40Ar/39Ar ages (Karlstrom et al., 2003); (2) 0-40 °C, 500-350 Ma: as documented by the Tonto Group and sub-Mississippian Redwall Limestone unconformities; (3) 50-150 °C, 90-70 Ma: due to deposition of 3-4 km of Mississippian to Cretaceous strata as documented by observed stratigraphic thicknesses in the Canyon and broader Colorado Plateau, as well as regional apatite (U-Th)/He and fission-track data (Flowers et al., 2008; Lee et al., 2013; Karlstrom et al., 2014); and (4) 0-40 °C, 1250 Ma: a fourth box was used where the Unkar Group is present in the eastern Grand Canyon or as a testing box to evaluate if the thermochronological data can resolve whether or not the Grand Canyon Supergroup was deposited in the western Grand Canyon.

# 4. RESULTS AND DISCUSSION

# 4.1. Zircon (U-Th)/He Date-eU Trends

The ZHe data consist of 102 single-aliquot dates from three studies (Peak et al., 2021; Thurston et al., 2022; this study; Table 1; Fig. S1). The combined data for the western Grand Canyon (Fig. 4A) show a single coherent, negative date-eU trend from 746 Ma to 69 Ma over a span of  $\sim$ 170 ppm eU to  $\sim$ 2000 ppm eU, with overlap and agreement of new dates collected in this study, and the previously published data of Peak et al. (2021). However, a single trend does not explain the combined data for the eastern Grand Canyon. Each contributing study occupies a different range of dates, with Peak et al. (2021) providing many of the Proterozoic ages, Thurston et al. (2022) providing all of the Cenozoic ages, and this study filling timeframes that overlap with Peak et al. (2021) and Thurston et al. (2022).

The marked difference in ages and the high amount of non-eU correlated dates between Peak et al. (2021) and Thurston et al. (2022) in the eastern Grand Canyon have several causes.

Peak et al. (2021) exhibited a difference in grainselection priority, with a preference for highly crystalline zircon, which typically records older ages, whereas Thurston et al. (2022) selected a wider range of grains that visually imply differences in radiation damage based on crystal color (Ault et al., 2018). The latter produced a wider range of dates, and the young (7-3 Ma) dates at high eU concentrations. Another notable difference is the assumption that all eastern Grand Canyon samples share a common thermal history, which is clearly less valid than perhaps is the case for western Grand Canyon samples. The absence of a single coherent date-eU trend for the entire eastern Grand Canyon data set supports this inference. Finally, sources of date dispersion other than radiation damage effects (e.g., zonation) may play a more important role than what we observe in the western Grand Canyon samples, but this cannot be verified. Despite the lack of a clear date-eU signal for the entire combined data set, a subset of ZHe dates has been influenced by accumulated radiation damage, as we observe young dates at inferred high damage levels (Thurston et al., 2022). This observation, combined with our goal of thoroughly assessing the resolving power of deep-time thermochronometers across the entire Grand Canyon, supports further investigation of the eastern Grand Canyon ZHe data in thermal history modeling, albeit with appropriate levels of skepticism where unambiguous date-eU trends are lacking.

The high date dispersion present in the ZHe data set (Fig. 4) is better interpreted by dividing the region into different domains, and even individual plutons, to identify meaningful dateeU trends. ZHe data from Grand Canyon basement (Peak et al., 2021; Thurston et al., 2022; and our new analyses) are subdivided into western (Fig. 4A) and eastern (Fig. 4B) segments. Western samples have dates that span from ca. 750 Ma to ca. 70 Ma over eU concentrations that range from 170 ppm to 1956 ppm in an overall negative trend. Eastern Grand Canyon data show a high degree of dispersion with dates that range from ca. 1325 Ma to ca. 3 Ma, with no clear trend related to eU. The complexity of the basement structure of the Grand Canyon lends itself to a variety of potential divisions, including division by major faults. In an attempt to resolve date-eU trends within these large and geographically separated data sets, we further subdivided the eastern and western data sets into basement domains delineated by shear zones previously defined by Holland et al. (2015). To reduce dispersion of the entire data set, we started with shear zones as domain boundaries where adjacent blocks have different Paleoproterozoic metamorphic histories (Robinson, 1994; Ilg et al., 1996; Dumond et al., 2007). Modeling of individual granitic plutons ensured a common thermal history for subsets of zircon grains. We also include a corresponding K-feldspar 40Ar/39Ar MDD analysis from each block. Figure 5 shows a cross section

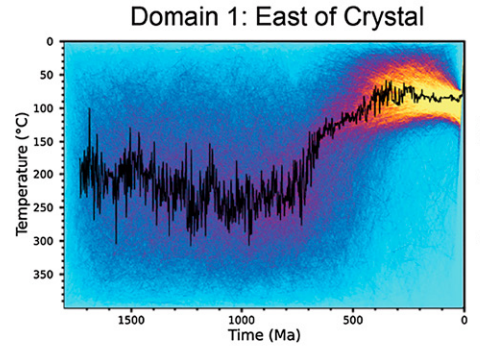
with these shear zones: the Crystal shear zone (river mile 98) and Gneiss Canyon shear zone (river mile 238). Negative slope date-eU trends are clearer for the easternmost and westernmost Domains 1 and 4, with Domains 2 and 3 showing more dispersion. Domain 1 (samples from east of the Crystal shear zone) zircon grains, from the Horn pluton, show oldest dates from 710 Ma to 291 Ma between 500 ppm eU and 1000 ppm eU plus dates as young 3.28 Ma at the highest eU. Domain 2 (samples from west of the Crystal shear zone) grains still show no clear date-eU trend, with ages varying from 800 Ma to 100 Ma across eU values ranging from 250 ppm to 750 ppm and no coherent date-eU trend. Therefore, modeling results based on ZRDAAM alone are suspect and shown only in the Supplemental Material (Fig. S10). Domain 3 (samples from east of the Gneiss Canyon shear zone) zircon grains are all from the Diamond Creek pluton; they show a dispersed date-eU negative trend. Domain 4 (samples from west of Gneiss Canyon shear zone) zircon grains show a tighter negative date-eU trend that includes grains from three plutons. We modeled subsets of grains from each of the four domains (Figs. 6-10).

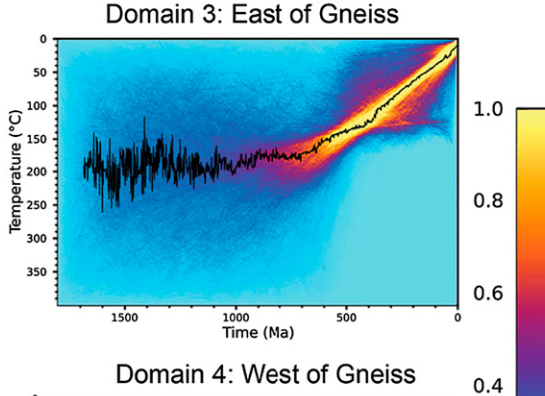
# **4.2.** Results of Thermal History Modeling Using QTQt: Sensitivity Testing

Figure 6 shows results from our ZHe-only models with no geologic constraint boxes for all

# Eastern Grand Canyon

# Western Grand Canyon





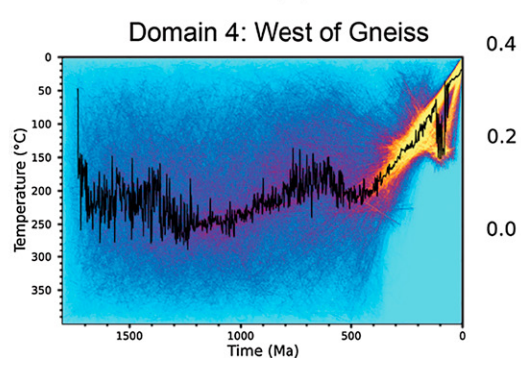


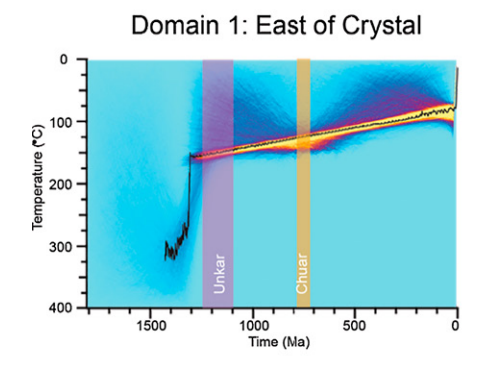
Figure 6. Summary of QTQt models that model all ZHe data for each section of the canyon with no constraint boxes; these model outputs should be viewed strictly in the context of sensitivity of the ZHe data to different portions of *t-T* space. In all panels, ZHe dates show almost no sensitivity to the Precambrian section of *t-T* space. That is, all segments have equally low relative probability in the Precambrian.

Relative Probability

Geological Society of America Bulletin

# Eastern Grand Canyon

# Western Grand Canyon



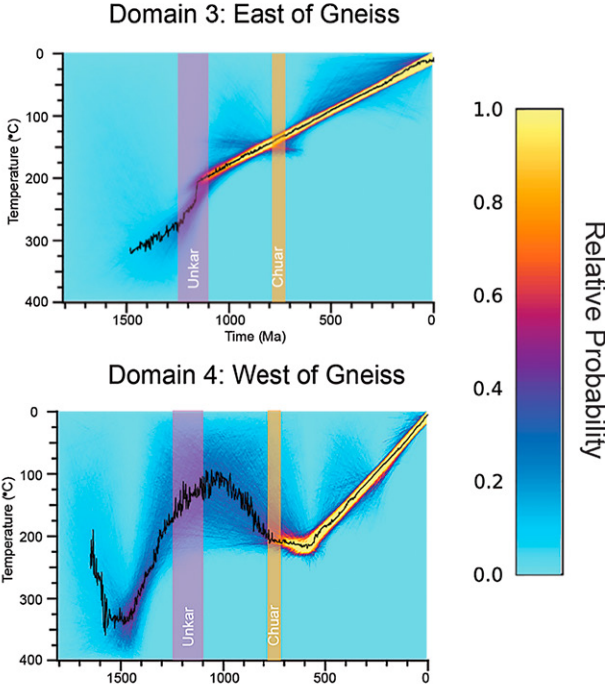


Figure 7. Summary of QTQt models that model all ZHe data and K-feldspar 40Ar/39Ar for each section of the canyon with no constraints. These model outputs should be viewed strictly in the context of sensitivity tests of the combined ZHe and K-feldspar 40Ar/39Ar data to different portions of t-T space. In all panels, combined data show sensitivity to a cooling segment between ca. 1350 Ma and 1250 Ma, but limited sensitivity onward; that is, post-1250 Ma segments of t-T space are either low probability or overly simplistic relative to the known geologic priors for the region. For specific sample locations for each datapoint, see Figure S2 (see text footnote 1).

subregions of the Grand Canyon. These outputs should be viewed only as sensitivity tests that attempt to quantify the *t-T* information inherent to the thermochronological data without incorporating additional model constraints (shown in other comparative models with incorporated geologic information). The purpose of this exercise is to clearly outline regions of the model space where the data contain t-T information and where the data may lack sensitivity. This is especially important when considering model-based thermal history interpretations that may or may not be entirely supported by geologic evidence. When inversions are shown with only applied constraint boxes (of varying quality or applicability), it is unclear whether the data are truly sensitive to or support such enforced constraints, or if this is simply a modeling consequence of the requirement for histories to pass through such boxes.

Regions of t-T space that have high-probability paths are only observed after ca. 500 Ma, with low-probability paths seen prior to 500 Ma. These results show that the ZHe data are not sensitive to the Proterozoic portion of the thermal history. Figure 7 shows the same model constraints with the addition of K-feldspar  $^{40}$ Ar/ $^{39}$ Ar data to each subregional data set. The models generated using both ZHe and K-feldspar  $^{40}$ Ar/ $^{39}$ Ar data show more constrained regions of high probability in the Precambrian. This suggests that the models are sensitive (i.e.,

the data contain some information) for this time span, and that co-modeling multiple chronometers, in this case specifically ZHe and K-feldspar 40Ar/39Ar, generates a higher resolution and therefore more probable deep-time thermal histories. The joint models without any geologic priors are still overly simplified when compared to the known geology, as is expected given the limited priors used, but several observations can still be drawn from this suite of models. Namely, we observe a dominant cooling segment starting at ca. 1350 Ma across all models. Also, Domain 1 (east of the Crystal shear zone) and Domain 4 (west of the Gneiss Canyon shear zone) models show lower probability regions that approach near-surface temperatures during the deposition of the Unkar Group. The observed ZHe ages and model-predicted ages fall variably within error of a one-to-one line, with some model outputs performing relatively well in matching observed to predicted ages, and others less so (Figs. S2-S6). In general, models that combine ZHe, 40Ar/39Ar, and modeling inputs are best able to match the observed to the predicted ages as inputs are best able to match the observed and predicted. There is a relatively high degree of mismatch between model and predicted ages for Domain 1 (Fig. S2), which may be due to the large discrepancy between relatively old (ca. 400 Ma) and very young (ca. 3 Ma) observed ages.

The QTQt ZHe-only models that use a minimum number of geologic constraint boxes

(Fig. 2B) are presented by domain from east to west in Figures 8D, 9D, and 10D. Figure 8D, from the easternmost Grand Canyon, shows a high-probability segment of the t-T paths at ~200 °C near the end of the Chuar Group deposition, similar to the HeFTy model. Figures 9D and 10D, from the western Grand Canyon, without the Unkar box, indicate that ZHe data alone contain very little information about the Proterozoic or early Phanerozoic history of this portion of the canyon-which suggests that nearly all zircon grains have been fully reset by Phanerozoic reheating. Indeed, all of our unconstrained ZHe-only models (Fig. 6) exhibit low-probability Precambrian t-T segments and an oscillating modal history (i.e., Maximum Mode path), which further suggests that the ZHe data alone provide little information about the 1250-500 Ma time period.

# 4.3. Results of K-Feldspar <sup>40</sup>Ar/<sup>39</sup>Ar MDD Thermal History Models

The K-feldspar sample locations are shown by stars in Figures 2 and 5 and represent one collected from each domain. All of the K-feldspar MDD age spectra are characterized by relatively young ages for the initial heating steps that climb steeply over the first 5%–10% of gas release to more gradual "staircase" patterns (e.g., Fig. 8B). In Domain 1, sample T0-86-2 shows an intermediate age hump for gas released over

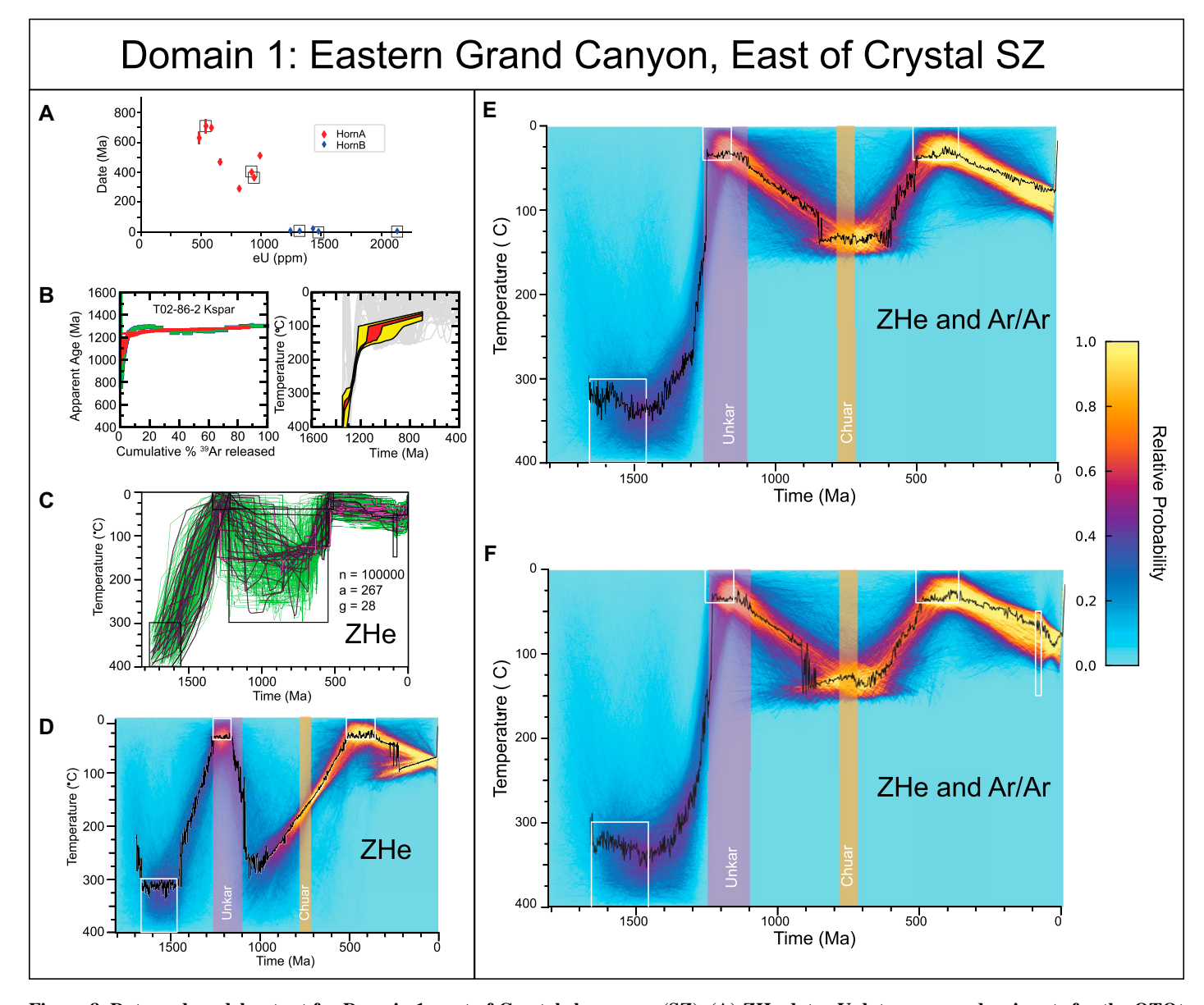


Figure 8. Data and model output for Domain 1: east of Crystal shear zone (SZ). (A) ZHe date-eU data were used as inputs for the QTQt models. Zircon grains used in HeFTy are highlighted with black rectangles. (B) K-feldspar <sup>40</sup>Ar/<sup>39</sup>Ar spectrum and multi-diffusion domain (MDD) model. (C) QTQt model output for ZHe using only Precambrian and Cambrian constraints (white boxes). (D) HeFTy model output, ZHe only, with all constraints. (E) QTQt model output for combined ZHe and K-feldspar <sup>40</sup>Ar/<sup>39</sup>Ar spectra with Precambrian and Cambrian constraints. (F) QTQt model output for combined ZHe and K-feldspar <sup>40</sup>Ar/<sup>39</sup>Ar data, with all constraints.

the 10%–40% range of the spectrum, with ages centered around 1225 Ma followed by a gradually climbing pattern from 1250 Ma to 1200 Ma. In Domain 3, sample H21-208.3a, a pegmatite that intrudes the Diamond Creek pluton, is principally characterized by an age gradient from ca. 1250 Ma to 1100 Ma over the final 90% of gas release (Fig. 9B) and is the youngest sample of the four reported results. In Domain 4, sample MH10-244.8b is dominated by ages older than 1350 Ma, with final step ages ca. 1450 Ma.

MDD-derived thermal histories are evaluated for cooling-only models (solid colors in

Figs. 8B, 9B, and 10B) as well as the more geologically realistic models that allow reheating (gray paths). These cooling-only models are commonly referred to as "monotonic cooling models," whereas the reheating models are commonly referred to as "unconstrained models," and neither model has imposed geologic constraint boxes. The monotonic thermal models do not extend to ages younger or older than those recorded by the age spectra measurements and thus are truncated to only show data given by the age-spectrum measurements. A common component of all of the <sup>40</sup>Ar/<sup>39</sup>Ar thermal histories

is that significant cooling from above 400  $^{\circ}$ C to  $\sim$ 200  $^{\circ}$ C occurred between ca. 1400 Ma and ca. 1300 Ma, with unconstrained models allowing cooling to the surface prior to Unkar deposition in both the eastern and western Grand Canyon.

In the western Grand Canyon (Figs. 9B and 10B), there is significant cooling from 1350 Ma to 1250 Ma, and unconstrained models allow exhumation to the surface by Unkar time; but, if so, samples need to be reheated to  $>200\,^{\circ}\text{C}$  by 1000 Ma (Figs. 9B and 10B) before cooling below 150 °C after 600 Ma. Thus, the MDD models permit the interpretation that the Unkar

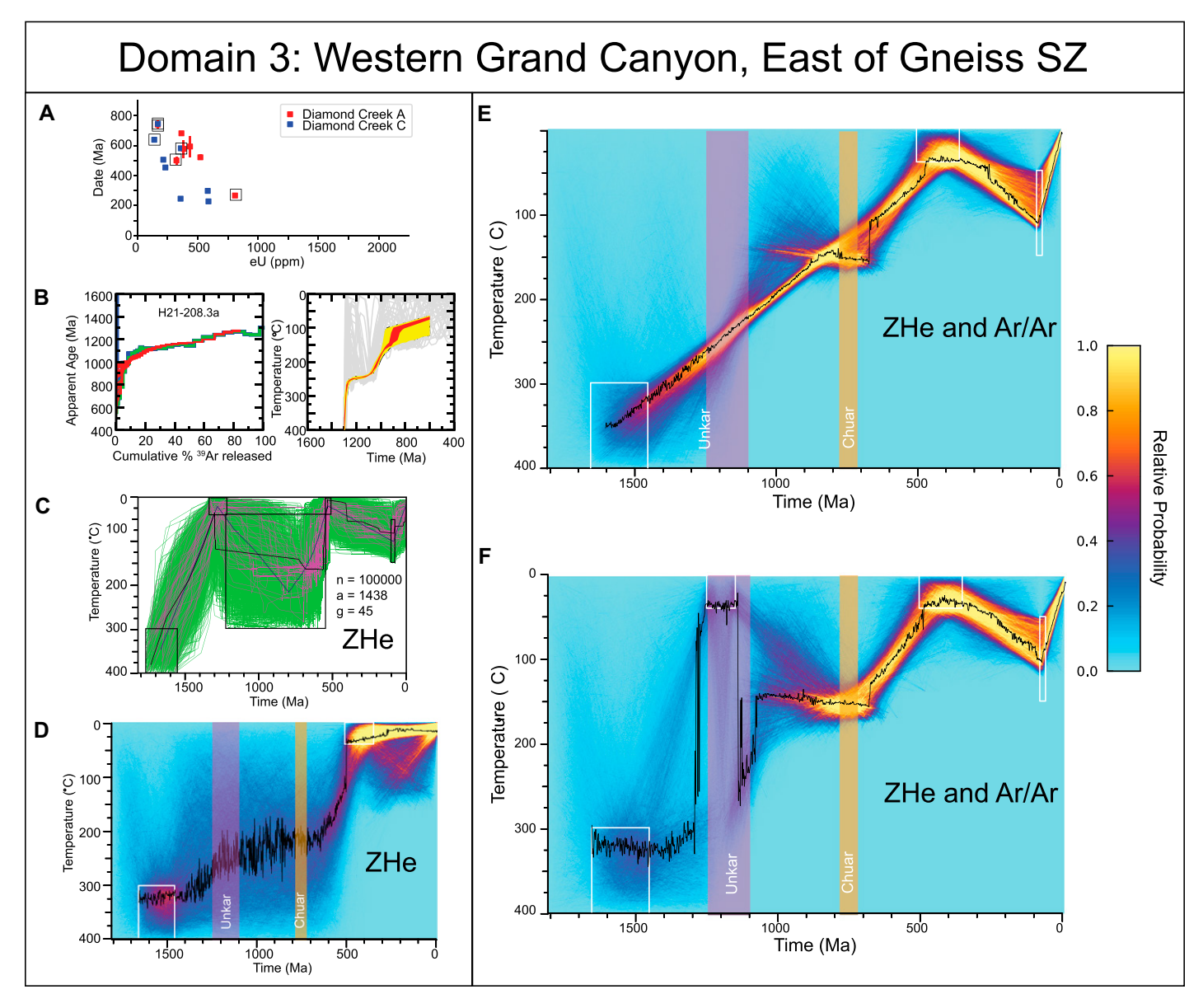


Figure 9. Data and model output for Domain 3: east of Gneiss Canyon shear zone (SZ). (A) ZHe date-eU spectrum used as inputs for the QTQt models; zircon grains used in HeFTy are highlighted with black rectangles. (B) K-feldspar <sup>40</sup>Ar/<sup>39</sup>Ar spectrum and multi-diffusion domain (MDD) model. (C) QTQt model output for ZHe only, with only Paleoproterozoic and Cambrian constraints. (D) HeFTy model output, ZHe only, with all constraints. (E) QTQt model output for combined ZHe and K-feldspar <sup>40</sup>Ar/<sup>39</sup>Ar spectra, with Precambrian and Cambrian constraints. (F) QTQt model output for combined ZHe and K-feldspar <sup>40</sup>Ar/<sup>39</sup>Ar spectra input, with test of the Unkar constraints.

Group was deposited in the western as well as eastern Grand Canyon but can equally support the interpretation that basement was not exhumed to the surface prior to 1250 Ma and remained deep and hot in the western Grand Canyon from 1250 Ma to 1100 Ma. Age spectra in all four domains record age gradients that extend into the Neoproterozoic. For cooling-only models, samples remained at 100 °C from ca. 1100 Ma to 800 Ma in the east (Fig. 8B) and 200 °C in the west (Fig. 9B). A later cooling event after 600 Ma is apparently recorded in the western, but not east-

ern, Grand Canyon, because samples T02-86-2 and T02-98-14 do not record apparent ages of less than ca. 900 Ma to 800 Ma. Thus, the details of cooling between 730 Ma and 500 Ma are not recorded by this particular thermochronometer.

# 4.4. Results of ZHe Thermal History Modeling Using HeFTy: Geologic Plausibility

Data subsets or averaged "synthetic ZHe dates" were modeled in previously published

papers. For a more direct comparison to previous results, this paper applies this same approach using the HeFTy software to grains from each of the four domains with minimal constraint boxes, as shown in Figure 2B. Similar to Peak et al. (2021), we use the "Unkar box" as a hypothesis test (between 1250 Ma and 500 Ma) to see if the ZHe data are compatible with deposition of the Grand Canyon Supergroup in the western Grand Canyon, such that its present absence may be due to a lack of preservation rather than nondeposition. We point out that the use of so-called

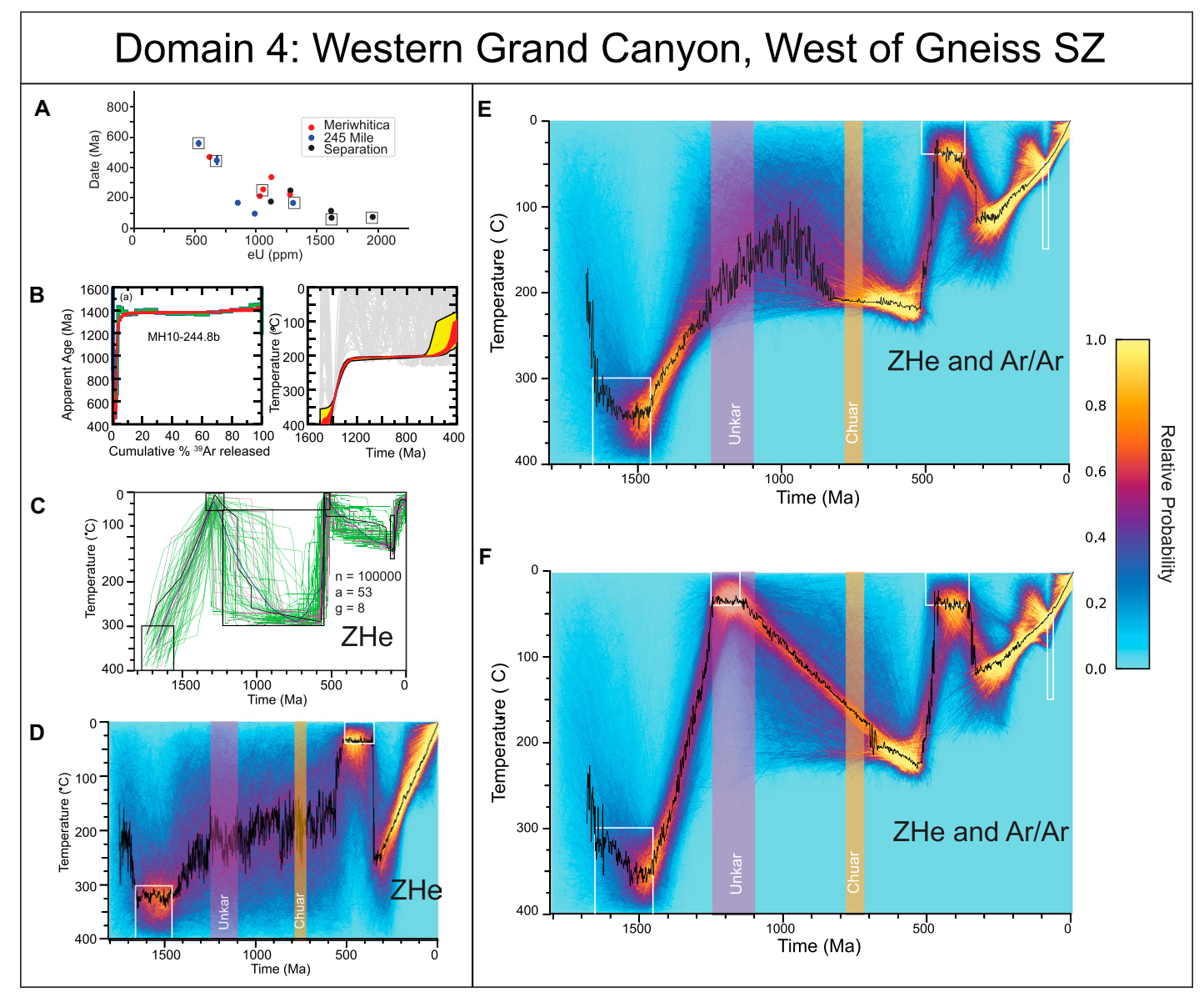


Figure 10. Data and model output for Domain 4: west of Gneiss Canyon shear zone (SZ) region. (A) ZHe date-eU were used as inputs for the QTQt models; zircon grains used in HeFTy are highlighted with black rectangles in the date-eU plot. (B) K-feldspar  $^{40}$ Ar/ $^{39}$ Ar spectrum and multi-diffusion domain model. (C) QTQt model output for ZHe only, with only Paleoproterozoic and Cambrian constraints. (D) HeFTy model output, ZHe only, with all constraints. (E) QTQt model output for combined ZHe and K-feldspar  $^{40}$ Ar/ $^{39}$ Ar spectra input, with test of the Unkar constraints.

"hypothesis test" constraint boxes truly tests the plausibility of a scenario only when the data actually are sensitive to an imposed model condition (e.g., McDannell et al., 2022c).

Domain 1 (Fig. 8C), for the easternmost Grand Canyon, is similar to the previously published HeFTy model from Thurston et al. (2022), but with fewer constraint boxes. The Domain 1 HeFTy model shows that the ZHe data allow many acceptable paths to describe the burial heating path associated with Grand Canyon Supergroup deposition and removal before the Cambrian. All eight good-fit paths at

the 0.5 significance level generated for Domain 1 show reheating during supergroup deposition to temperatures of >250 °C. The weighted mean of the path for Domain 1 predicts that basement rocks were heated to  $\sim$ 175 °C by the end of Chuar deposition at 729 Ma. This is  $\sim$ 50 °C higher than the "predicted" burial heating shown in Figure 2B caused by  $\sim$ 4 km ( $\sim$ 100 °C) of Grand Canyon Supergroup deposition by 729 Ma (Karlstrom et al., 2021). However, as discussed above, the ZHe data are relatively insensitive to Neoproterozoic portions of *t-T* space due to reheating in the Mesozoic and

Cenozoic (i.e., prior to the Laramide orogeny), so this variability in maximum temperature is expected. The Cambrian geologic constraint box dictates basement cooling to the near-surface by 508 Ma, and the model allows a variety of paths, with a weighted mean path remaining >100 °C until after 600 Ma. The HeFTy model results for the western Grand Canyon, Domain 3 (Fig. 9C) and Domain 4 (Fig. 10C), have very similar results and suggest that the highest temperatures were reached near Chuar time followed by rapid cooling from 600 Ma to 500 Ma. The individual good-fitting paths for Domain 3

Figure 11. (A) Summary of QTQt models that jointly model all ZHe data with K-feldspar <sup>40</sup>Ar/<sup>39</sup>Ar. Domain 1: eastern Grand Canyon models use unequivocal geologic constraints. Domains 3 and 4: western Grand Canyon models test the Unkar box and find that thermochronological data are compatible with (but do not prove) published models that the Grand Canyon Supergroup could have been deposited and then eroded. (B) QTQt forward models from jointly modeled ZHe and K-feldspar <sup>40</sup>Ar/<sup>39</sup>Ar data. (I) Cooling paths without the Unkar constraint can produce (II) K-feldspar multi-diffusion domain (MDD) release spectra and (III) negative age-Eu trends resembling Grand Canyon data. (IV) Cooling paths using the Unkar box can also produce (V) K-feldspar MDD release spectra and (VI) negative date-eU trends resembling Grand Canyon data. See text and Supplemental Text S2 (see text footnote 1) and associated figures for further discussion.

and Domain 4 overwhelmingly show reheating during Supergroup deposition, with only two good paths from Domain 3 showing no reheating from 1250 Ma to 600 Ma. Our ZHe HeFTy results for the western Grand Canyon, which include the Peak et al. (2021) data, are equally compatible with nondeposition or deposition of the Unkar and Chuar groups across the western Grand Canyon region.

# 4.5. Results of ZHe + $^{40}$ Ar/ $^{39}$ Ar MDD K-feldspar Thermal History Modeling Using QTQt

Using QTQt to co-model both ZHe and  $^{40}$ Ar/ $^{39}$ Ar K-feldspar data, we tested several models using unequivocal geologic constraint boxes to further evaluate the likelihood of certain t-T scenarios. For the easternmost Grand Canyon, Domain 1, Figures 8E and 6F show a high probability for maximum temperatures of  $\sim$ 150  $^{\circ}$ C at 800–650 Ma with rapid cooling after ca. 600 Ma. Adding a pre-Laramide maximum burial constraint in Figure 6F makes little difference to the models, which suggests that the data are sensitive to the Cenozoic part of the thermal history.

Western Grand Canyon joint models include the unequivocal constraints (Figs. 9E and 10E), as well as an Unkar box (Figs. 9F and 10F), to test its effect, similar to the approach of Peak et al. (2021), but with more data from two integrated thermochronometric systems. Figure 9E, without the Unkar box, produces paths similar to the monotonic cooling 40Ar/39Ar K-feldspar MDD model (Fig. 9B) and the combined K-feldspar 40Ar/39Ar and ZHe model without constraints (Fig. 7B). Paths show largely "linear" (i.e., low-complexity) monotonic cooling; however, some lower likelihood paths are compatible with near-surface temperatures and reheating before Chuar time. It is important to note that linear monotonic results in QTQt do not preclude the possibility of more complex t-T paths. That is, the 40Ar/39Ar K-feldspar data contain some information about the Proterozoic thermal history of these samples, as opposed to the ZHe data alone, which only show diffuse, lowprobability paths in QTQt output. However, even the 40Ar/39Ar K-feldspar data, in this particular

case, cannot resolve higher complexity solutions in the absence of additional geologic data due to temperature sensitivity limits. The addition of an Unkar depositional constraint (Fig. 9F) naturally yields more complex paths. The westernmost Grand Canyon (Domain 4) models in Figure 8E exhibit diffuse low probabilities with an irregular Maximum Mode *t-T* path from 1250 Ma to 600 Ma that permits, but does not require, Grand Canyon Supergroup deposition.

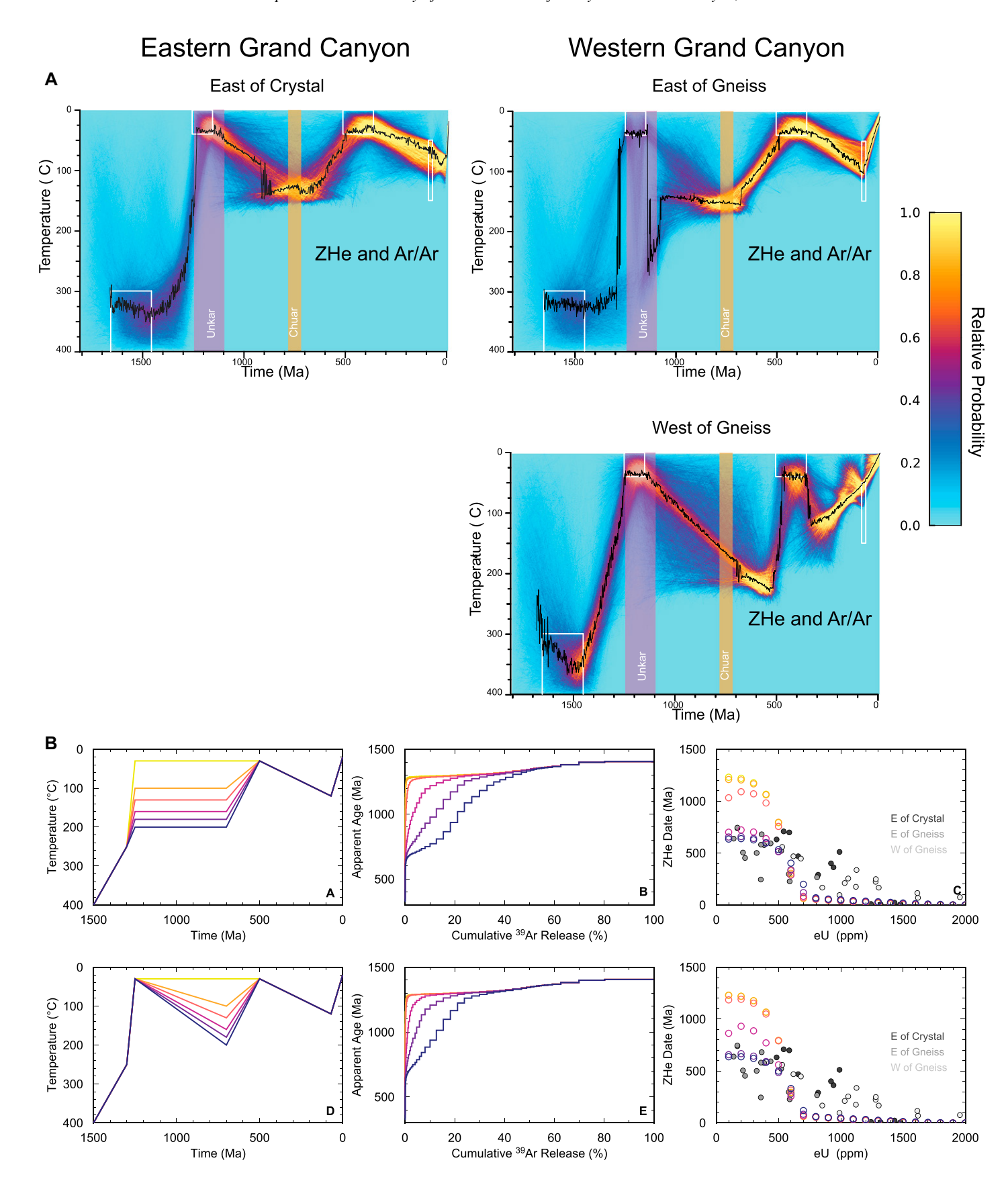
# **4.6. Forward Models of Grand Canyon Histories**

We further illustrate the t-T sensitivity limitations apparent in all currently published Grand Canyon ZHe thermochronometry using forward thermal history modeling. Forward models use a specified set of parameters (i.e., input t-T history and idealized thermochronometric data/kinetics) to predict synthetic thermochronological data. This process assists in understanding the significance and sensitivity of real chronometric data. This differs from inverse modeling, where we are identifying a suite of thermal histories that accurately reproduce observed thermochronological data within uncertainty. The real thermal history and our observed K-feldspar MDD and ZHe results are more nuanced and typically contain more "geological scatter" than can be captured with a simple forward model, and therefore necessitate a formal inversion. Nonetheless, we are determining whether certain styles (or parts) of a thermal history produce meaningful or interpretable data trends that then bear on the sensitivity of our real thermochronometric data.

Thermal histories were forward modeled using the MDD code *ages.f* (Lovera, 1992; https://github.com/OpenThermochronology for details) and the ZRDAAM code from Guenthner et al. (2013) to predict K-feldspar <sup>40</sup>Ar/<sup>39</sup>Ar MDD age spectra and ZHe date-eU trends akin to the real data collected in the Grand Canyon. The modeling methods are the same as those discussed in McDannell and Flowers (2020). The synthetic thermochronological data used as inputs were a typical Grand Canyon K-feldspar with nine diffusion domains and activation energy of ∼192 kJ/mol (46 kcal/mol) and ZHe dates spanning 100–2000 ppm eU with a fixed

spherical grain radius of  $50~\mu m$ . In our hypothetical Grand Canyon forward model scenarios, only the Proterozoic history was changed, and comparisons were made between (1) Proterozoic paths of solely monotonic cooling that did not include an explicit surface constraint at the timing of Unkar deposition and (2) reheating-type histories with an Unkar surface constraint at 1250~Ma.

The forward models (Fig. 11B) show nearly identical ZHe date-eU trends and K-feldspar <sup>40</sup>Ar/<sup>39</sup>Ar spectra whether the basement surface is held at elevated temperature (i.e., Peak et al., 2021), or if it is exhumed and reheated, which is consistent with Grand Canyon Supergroup deposition. In detail, high-quality K-feldspar MDD age spectra may be able to distinguish between simplistic reheating or monotonic-cooling endmember histories within an inversion. In practice, this is dependent upon the sample diffusion kinetics and the domain distribution. Another complicating factor is that the t-T information provided by the early laboratory heating steps (i.e., smallest diffusion domains and youngest step ages) is often obscured by fluid inclusionderived excess Ar (e.g., Harrison et al., 1994). Nonetheless, the predicted ZHe dates match the first-order date-eU patterns found in the observed data-even though the real ZHe dates exhibit excess age dispersion that is not well explained. Cooler middle-late Proterozoic temperatures between 20 °C and 160 °C produce much older model ZHe dates between ca. 1200 Ma and 800 Ma at low eU conditions that are not present in the real ZHe data set, which implies that elevated temperatures are required to explain the real ZHe dates. These subtle features of the synthetic data set tell us that the real ZHe dates can be explained by either thermal resetting via deep-burial reheating or monotonic cooling through apparent closure temperatures in the late Neoproterozoic. Importantly, our forward models demonstrate that both monotonic and reheating scenarios produce similar predicted MDD and ZHe data and require basement rocks at elevated temperatures of >160 °C in the late Neoproterozoic. Thus, the currently published catalog of Grand Canyon ZHe data in isolation is not sensitive to near-surface conditions at 1250 Ma during Unkar Group deposition, such that



the combined models are strongly influenced by the  $^{40}$ Ar/ $^{39}$ Ar data for the 1350–1250 Ma cooling episode. Figures 8E and 8F both show high probability of  $\sim$ 180–200 °C temperatures ca. 700 Ma prior to rapid cooling between 600 Ma and 500 Ma.

## 5. INTERPRETATION

#### 5.1. Interpretation of Thermochronology

The combined ZHe and K-feldspar 40Ar/39Ar data with unequivocal geological priors in QTQt provide the most robust models (Figs. 8F, 9F, and 10F). All other models discussed here and in the previous sections, such as the ZHe-only models run in both HeFTy and QTQt, show generally less *t-T* resolution for certain timeframes (e.g., 1250-500 Ma) and should be viewed as sensitivity tests of the various data used in our modeling exercises (ZHe, K-feldspar 40Ar/39Ar, and geologic data). That is, we evaluate the strength of our geologic interpretations based on the available data in the context of all of the models, not merely a subset. Several consistent observations emerge from this approach: (1) in the eastern Grand Canyon, where the Unkar constraint box is unquestionable, the combined ZHe and <sup>40</sup>Ar/<sup>39</sup>Ar K-feldspar models (Figs. 8F) showed that reheating segments are required to predict both sets of data; (2) 40Ar/39Ar K-feldspar data support the interpretation that 1350-1250 Ma cooling was the first and main episode of basement cooling throughout the Grand Canyon; and (3) the two thermochronometers combined show an interval of cooling from maximum temperatures between 100 °C and 200 °C to surface temperatures between ca. 600 Ma and 500 Ma, which is best recorded in Domains 1, 3, and 4. To better quantify the late cooling episode, we calculated the timing of peak cooling in the late Neoproterozoic to Early Cambrian for these three domains using the "full time-distribution at half-maximum temperature" (FDHM) method discussed in McDannell and Keller (2022; https://github.com/OpenThermochronology/CoolingFDHM). This approach examines all of the cooling paths within a specific time window, which was 750-508 Ma for Domains 1 and 3, and 600-508 Ma for Domain 4. The half-maximum isotherm of the total cooling path is accepted as the peak cooling within the interval. The times in the t-T model when those paths cross the isotherm are linearly interpolated (1 m.y. step) to provide a full temporal distribution at the half-maximum temperature. Domain 1 exhibits  $\sim$ 150 °C of total cooling with the 75 °C isotherm being the half-maximum; Domain 3 exhibits  $\sim$ 170 °C of total cooling with the 85 °C isotherm being the half-maximum; and

Domain 4 shows  $\sim$ 238 °C of total cooling with a half-maximum isotherm of 119 °C. The time of peak cooling for each respective domain is: 526 + 51/-6 Ma (Domain 1), 573 + 33/-33 Ma (Domain 3), and 510 + 16/-3 Ma (Domain 4). We emphasize that for Domain 4, total reheating/cooling magnitude and the timing of peak cooling are strongly influenced by the early <sup>39</sup>Ar step-release of the K-feldspar sample (<2% cumulative gas) and should be cautiously interpreted. Within the limits of the current integrated thermochronological data sets, the peak cooling interval in the Neoproterozoic is between ca. 606 Ma and 507 Ma in the Grand Canyon domains studied here.

A comparison of the three modeled domains of the combined ZHe and 40Ar/39Ar K-feldspar results is shown in Figure 11. These outputs yield relatively high path densities (i.e., probabilities) for regions of t-T space that are consistent with Grand Canyon Supergroup deposition in both the eastern and western regions of the Grand Canyon. Domains 1 and 4 are the best resolved by the combined models and suggest the possibility of similar, though not identical, thermal histories across the entire Grand Canyon transect. For the eastern Grand Canyon, Domain 1 shows what we interpret to be the most statistically and geologically probable t-T path, with maximum temperatures of ~150 °C reached at ca. 700 Ma, which is consistent with the observed 4 km of Grand Canyon Supergroup in Domain 1, followed by cooling to surface temperatures after ca. 600 Ma. Though this is the best model for the eastern Grand Canyon, the models remain insensitive to the smaller unconformities that punctuate Unkar and Chuar strata and the Mississippian and Permian strata. Western Grand Canyon models with and without the Unkar constraint box both give variably complex (depending on priors used) but equally permissible models, and hence do not constrain the original presence, absence, or thickness of the Grand Canyon Supergroup in the western Grand Canyon. However, models from Domains 3 and 4 suggest basement temperatures of  $\sim$ 150–200 °C from 600 Ma to 500 Ma prior to cooling at ca. 500 Ma. Whether this 5-8 km of now-removed material was basement and/or Grand Canyon Supergroup sedimentary cover (as is the case in the eastern Grand Canyon) is not constrained by the thermochronological data.

Forward models (Fig. 11B) demonstrate multiple *t-T* path scenarios and the corresponding <sup>40</sup>Ar/<sup>39</sup>Ar K-feldspar MDD age spectra and ZHe date-eU trends predicted by such paths. These models confirm the inverse modeling in showing that the thermochronological data are compatible with or without the Unkar constraint and cannot distinguish whether the Grand Canyon

Supergroup was deposited in either the eastern or western Grand Canyon. For all of the structural domains, models show that ZHe data are sensitive to the Phanerozoic thermal history and canyon incision (Thurston et al., 2022). For Domain 1, where only D, E, and F in Figure 8 are geologically reasonable, the 40Ar/39Ar age spectrum of Figure 8 is best matched by pre-600 Ma basement temperatures of  $\sim$ 120–140 °C (burial by 4–5 km of strata), whereas the observed maximum ZHe ages of ca. 700 Ma at low eU conditions are best predicted by pre-600 Ma basement temperatures of  $\sim$ 150 °C. Both of these scenarios suggest that the ~4 km of preserved thickness of the Grand Canyon Supergroup in the eastern Grand Canyon may be most of the 4-5 km original thickness. Domain 4 in the western Grand Canyon gives similar results to Domain 1. Forward models also show that basement temperatures of <100 °C at 600 Ma would predict ZHe ages older than 1.0 Ga, which are not observed in eastern or western Grand Canyon data sets and suggests that the basement was likely still >3-4 km deep across the transect at 600 Ma.

## 5.2. Interpretation of Geology

The major cooling trend from 1350 Ma to 1250 Ma is present in the easternmost and westernmost Grand Canyon (compare Figs. 8A and 10D and all models that include 40Ar/39Ar data). Neither thermochronological nor geologic data resolve the original extent and thickness of the Grand Canyon Supergroup across the western Grand Canyon region. However, Unkar Group carbonates (Bass Formation) have been correlated regionally, which suggests a potentially broad basin geometry (Timmons et al., 2005; Mulder et al., 2017). The 1.1 Ga diabase intrusions are also present in the eastern and western Grand Canyon and throughout the southwestern Laurentian region (Howard, 1991; Mohr et al., 2024). Their depth of emplacement is unknown, but diabase sills in the eastern Grand Canyon are thicker, more voluminous, and coarser; thus, there is no reason to postulate that the western diabase intrusions were deeper.

The Chuar Group has been correlated to Death Valley (Mahon et. al., 2014), the Uinta Mountain Group of Utah, USA (Dehler et al., 2017), and northernmost Idaho, USA (Brennan et al., 2020), using lithologic correlations, detrital zircons, and chemostratigraphy. The sedimentary units are fine-grained and dominantly marine based on cosmopolitan microfossils (Porter, 2016). Facies distributions indicate that the basins extended well beyond their present extent. Dehler et al. (2017) used the term ChUMP basin for the proposed once-contiguous, dominantly shallow-marine succession deposited regionally

at 775–729 Ma. This differs from a model of a localized and isolated Tonian basin in southwestern Laurentia (i.e., Peak et al., 2021).

Western Grand Canyon Domains 3 and 4 show basement temperatures after 729 Ma to have been  $\sim 150-200$  °C with or without the Unkar constraint box, which suggests that the basement could have been 2-4 km deeper in the western Grand Canyon than in the eastern portion. One plausible mechanism to explain this heating is deposition of an additional 2-4 km of Neoproterozoic and Lower Cambrian strata west of the Cordilleran passive margin hingeline (Yonkee et al., 2014; Nelson et al., 2020). Modeled final unroofing of basement in Domains 1, 3, and 4 (and likely across the entire transect) to the surface at 600–500 Ma, guided by the limited number but critically important low-eU 600-500 Ma ZHe dates, is thus interpreted to be related to regional ca. 508 Ma Cambrian tectonism (Karlstrom et al., 2018).

Present thermochronological data do not resolve differences across the numerous fault blocks (Fig. 3). We attribute this to the lack of strategic sampling for combined ZHe and K-feldspar 40Ar/39Ar analysis on the same samples. At present, we do not know the extent to which differences in thermal histories shown in Figure 11 may reflect low resolution of the thermochronometers for certain parts of t-T space (i.e., ZHe in the Precambrian) or true differences in thermal history related to the geology. Except for a few 600-500 Ma dates, many of the ZHe grains are thermally reset and predominantly record Mesozoic burial. A more targeted sampling approach that minimizes the effects of Phanerozoic reheating could prove valuable for investigating more local-scale differences in thermal histories. For example, Figure 5 uses dashed lines to show some Cenozoic faults that may have been reactivated from the NE, NW, and N-S Precambrian trends, such as the ca. 750 Ma Butte fault, which is interpreted as an inboard expression of Rodinia rifting (Karlstrom et al., 2001) with  $\sim$ 2 km of Precambrian throw. The Sinyala fault, postulated by Peak et al. (2021, their fig. 4) to have bounded an uplifted western Grand Canyon block at time slices of 1250 Ma and 800 Ma, is a Neogene normal fault with only meters of slip (Huntoon et al., 1996) and no known earlier ancestry. Differences in thermal history could manifest even within some sample domains, such as Domain 1; there, even though the samples come from a single pluton, the K-feldspar sample is from a few river miles upstream of the zircon sample across the Bright Angel and Vishnu faults. For Domain 3, the 1.73 Ga Diamond Creek pluton was sampled in two places, and the K-feldspar sample came from a younger (ca. 1.7 Ga) pegmatite several

miles upstream. In the future, detailed sampling approaches could explore the potential thermal history differences across these faults.

# 6. NATURE OF THE GREAT UNCONFORMITY

Geologically, it has long been clear that there were multiple episodes of basement unroofing in the Grand Canyon (Powell, 1876; Karlstrom and Timmons, 2012a). Thermochronological evidence suggests ~100-300 °C of cooling between 1350 Ma and 1250 Ma and 150-200 °C of cooling between 600 Ma and 500 Ma in all areas of the canyon, with the latter leading to the Middle Cambrian marine transgression that produced the final expression of the Great Unconformity. Grand Canyon thermal history models do not produce high-probability path segments that overlap with 717-635 Ma cooling due to kilometer-scale glacial erosion during the Snowball Earth (Keller et al., 2019). Local tectonic unroofing, however, does not invalidate a continental-scale glacial erosion model (McDannell et al., 2022a; McDannell and Keller, 2022). In addition, a recently proposed late Ediacaran ice age (580-560 Ma) has been recognized globally and across Laurentia (Wang et al., 2023), which may complicate determination of the cause of unroofing in the Grand Canyon. A new contribution of this paper is that the basement for the entire Grand Canyon region appears to have been unroofed by several kilometers between ca. 600 Ma and 500 Ma. Overall, current thermochronological data are not sensitive enough to parse the scale of additional differential basement cooling events that must have taken place in uplifting blocks during early Unkar deposition at 1250-1200 Ma, or between ca. 1100 Ma and ca. 775 Ma (Thurston et al., 2022), nor during Phanerozoic reactivations of older faults.

For Laurentia and perhaps globally, the nature and significance of the Great Unconformity has received recent attention. Grand Canyon data do not readily support the hypothesis that the Great Unconformity was causally linked, globally, to the Cambrian explosion of animal life (Peters and Gaines, 2012) because the post-508 Ma sheet sandstones of the overlying basement of the Tapeats Sandstone are  $\sim$ 10 m.y. younger than the appearance of shelled fossils (Karlstrom et al., 2020). The absence of a significant regolith at this contact (Sharp, 1940) possibly suggests that Cambrian transgression and sandstone deposition starting after 508 Ma closely followed a post-600 Ma basement unroofing event. Models for deep-basement erosion during ca. 1100 Ma assembly and ca. 750 Ma breakup of Rodinia (DeLucia et al., 2018; Flowers et al., 2020) do not match well with the main ca. 1350-1250 Ma and ca. 600–500 Ma cooling pulses modeled for the Grand Canyon.

# 7. CONCLUSIONS

Jointly modeled, multiple deep-time thermochronometric data sets advance several discussions related to the Precambrian thermal history of the Grand Canyon and the origin of the Great Unconformity. We demonstrated that the joint inversion of ZHe and K-feldspar 40Ar/39Ar models produces more resolved Precambrian t-T paths than ZHe or K-feldspar  $^{40}\text{Ar}/^{39}\text{Ar}$  data alone. In both the western and eastern portions of the Grand Canyon, thermochronological modeling supports two main basement cooling events at ca. 1350-1250 Ma and ca. 600-500 Ma. Basement cooling to surface temperatures by ca. 1250 Ma and deposition of the Grand Canyon Supergroup seem likely in the western Grand Canyon, as modeling results from the western Grand Canyon data set show equal probability of paths that can reach the surface by 1250 Ma, or remain at elevated temperatures (150-200 °C), and all models suggest the basement was at 150-200 °C (5-8 km deep) until rapid exhumation to the surface between 600 Ma and 500 Ma. In the Grand Canyon, the term "Great Unconformity" is used to refer to the contact between crystalline basement and Cambrian Tapeats Sandstone. The main >10 km basement exhumation event occurred at 1350-1250 Ma during the erosional demise of 1700-1400 Ma high topography of the Vishnu Mountains to create the sub-Bass unconformity. The sub-Tapeats unconformity is expressed both as an angular unconformity where it bevels across remnants of the Mesoproterozoic Unkar Group and Neoproterozoic Chuar Group (Fig. 3B), and as an unconformity where Tapeats Sandstone rests on the basement. In both expressions, the last erosional episode was in the Middle Cambrian (ca. 508 Ma; Karlstrom et al., 2018) as part of a 600-500 Ma regional basement exhumation event.

# ACKNOWLEDGMENTS

W.R. Guenthner acknowledges National Science Foundation Division of Earth Sciences (NSF-EAR) grant nos. 1735788 and 1848013. K.E. Karlstrom acknowledges NSF-EAR grant no. 1348007. K.E. Karlstrom and M.T. Heizler acknowledge NSF-EAR grant no. 9902955. Grand Canyon National Park provided collecting permits to K.E. Karlstrom. We thank two anonymous reviewers for helpful comments that improved this manuscript.

#### REFERENCES CITED

Ault, A.K., Guenthner, W.R., Moser, A.C., Miller, G.H., and Refsnider, K.A., 2018, Zircon grain selection reveals (de) coupled metamictization, radiation damage, and He diffusivity: Chemical Geology, v. 490, p. 1–12, https://doi.org/10.1016/j.chemgeo.2018.04.023.

- Brennan, D.T., Pearson, D.M., Link, P.K., and Chamberlain, K.R., 2020, Neoproterozoic Windermere Supergroup near Bayhorse, Idaho: Late-stage Rodinian rifting was deflected west around the Belt basin: Tectonics, v. 39, https://doi.org/10.1029/2020TC006145.
- Dehler, C., Gehrels, G., Porter, S., Heizler, M., Karlstrom, K.E., Cox, G., Crossey, L.C., and Timmons, J.M., 2017, Synthesis of the 780–740 Ma Chuar, Uinta Mountain, and Pahrump groups (ChUMP), western USA: Implications for Laurentia-wide cratonic marine basins: Geological Society of America Bulletin, v. 129, p. 607–624, https://doi.org/10.1130/B31532.1.
- DeLucia, M.S., Guenthner, W.R., Marshak, S., Thomson, S.N., and Ault, A.K., 2018, Thermochronology links denudation of the Great Unconformity surface to the supercontinent cycle and snowball Earth: Geology, v. 46, p. 167–170, https://doi.org/10.1130/G39525.1.
- Dumond, G., Mahan, K.H., Williams, M.L., and Karlstrom, K.E., 2007, Crustal segmentation, composite looping pressure-temperature paths, and magma-enhanced metamorphic field gradients: Upper Granite Gorge, Grand Canyon, USA: Geological Society of America Bulletin, v. 119, p. 202–220, https://doi.org/10.1130/B25903.1.
- Dutton, C.E., 1882, Tertiary history of the Grand Canyon district: American Journal of Science, v. S3-24, p. 81–89, https://doi.org/10.2475/ajs.s3-24.140.81.
- Flowers, R.M., and Farley, K.A., 2012, Apatite <sup>4</sup>He/<sup>3</sup>He and (U-Th)/He evidence for an ancient Grand Canyon: Science, v. 338, p. 1616–1619, https://doi.org/10.1126/science.1229390.
- Flowers, R.M., and Kelley, S.A., 2011, Interpreting data dispersion and "inverted" dates in apatite (U-Th)/He and fission-track datasets: An example from the US mid-continent: Geochimica et Cosmochimica Acta, v. 75, p. 5169–5186, https://doi.org/10.1016/j.gca.2011.06.016.
- Flowers, R.M., Wernicke, B.P., and Farley, K.A., 2008, Unroofing, incision, and uplift history of the southwestern Colorado Plateau from apatite (U-Th)/He thermochronometry: Geological Society of America Bulletin, v. 120, p. 571–587, https://doi.org/10.1130/B26231.1.
- Flowers, R.M., Macdonald, F.A., Siddoway, C.S., and Havranek, R., 2020, Diachronous development of great unconformities before Neoproterozoic snowball Earth: Proceedings of the National Academy of Sciences of the United States of America, v. 117, p. 10,172–10,180, https://doi.org/10.1073/pnas.1913131117.
- Flowers, R.M., Zeitler, P.K., Danišík, M., Reiners, P.W., Gautheron, C., Ketcham, R.A., Metcalf, J.R., Stockli, D.F., Enkelmann, E., and Brown, R.W., 2023, (U-Th)/He chronology: Part 1. Data, uncertainty, and reporting: Geological Society of America Bulletin, v. 135, p. 104–136, https://doi.org/10.1130/B36266.1.
- Gallagher, K., 2012, Transdimensional inverse thermal history modeling for quantitative thermochronology: Journal of Geophysical Research: Solid Earth, v. 117, https://doi.org/10.1029/2011JB008825.
- Ginster, U., Reiners, P.W., Nasdala, L., and Chanmuang, C., 2019, Annealing kinetics of radiation damage in zircon: Geochimica et Cosmochimica Acta, v. 249, p. 225–246, https://doi.org/10.1016/j.gca.2019.01.033.
- Gleadow, A., Harrison, M., Kohn, B., Lugo-Zazueta, R., and Phillips, D., 2015, The Fish Canyon Tuff: A new look at an old low-temperature thermochronology standard: Earth and Planetary Science Letters, v. 424, p. 95–108, https://doi.org/10.1016/j.epsl.2015.05.003.
- Guenthner, W.R., 2021, Implementation of an alpha damage annealing model for zircon (U-Th)/He thermochronology with comparison to a zircon fission track annealing model: Geochemistry, Geophysics, Geosystems, v. 22, no. 2, https://doi.org/10.1016/j.chemgeo.2024.121949.
- Guenthner, W.R., Reiners, P.W., Ketcham, R.A., Nasdala, L., and Giester, G., 2013, Helium diffusion in natural zircon: Radiation damage, anisotropy, and the interpretation of zircon (U-Th)/He thermochronology: American Journal of Science, v. 313, p. 145–198, https://doi.org /10.2475/03.2013.01.
- Guenthner, W.R., Reiners, P.W., and Chowdhury, U., 2016, Isotope dilution analysis of Ca and Zr in apatite and zircon (U-Th)/He chronometry: Geochemistry, Geophysics, Geosystems, v. 17, p. 1623–1640, https://doi.org/10 .1002/2016GC006311.

- Harrison, M.T., Heizler, M.T., Lovera, O.M., Chen, W., and Grove, M., 1994, A chlorine disinfectant for excess argon released from K-feldspar during step heating: Earth and Planetary Science Letters, v. 123, p. 95–104, https://doi.org/10.1016/0012-821X(94)90260-7.
- Holland, M.E., Karlstrom, K.E., Doe, M.F., Gehrels, G.E., Pecha, M., Shufeldt, O.P., Begg, G., Griffin, W.L., and Belousova, E., 2015, An imbricate midcrustal suture zone: The Mojave-Yavapai province boundary in Grand Canyon, Arizona: Geological Society of America Bulletin, v. 127, p. 1391–1410, https://doi.org/10.1130 //B31232.1.
- Hourigan, J.K., Reiners, P.W., and Brandon, M.T., 2005, U-Th zonation-dependent alpha-ejection in (U-Th)/He chronometry: Geochimica et Cosmochimica Acta, v. 69, p. 3349–3365, https://doi.org/10.1016/j.gca .2005.01.024.
- Howard, K.A., 1991, Intrusion of horizontal dikes: Tectonic significance of middle Proterozoic diabase sheets widespread in the upper crust of the southwestern United States: Journal of Geophysical Research: Solid Earth, v. 96, p. 12,461–12,478, https://doi.org/10.1029/91JB00112.
- Huntoon, P., Billingsley, G.H., Sears, J.W., Ilg, B.R., and Karlstrom, K.E., 1996, Geologic map of the eastern part of the Grand Canyon National Park: Grand Canyon Natural History Association, scale 1:62,500, 1 sheet.
- Ilg, B.R., Karlstrom, K.E., Hawkins, D.P., and Williams, M.L., 1996, Tectonic evolution of Paleoproterozoic rocks in the Grand Canyon: Insights into middlecrustal processes: Geological Society of America Bulletin, v. 108, p. 1149–1166, https://doi.org/10.1130 //0016-7606(1996)108<1149:TEOPRI>2.3.CO;2.
- Kaempfer, J.M., Guenthner, W.R., and Pearson, D.M., 2021, Proterozoic to Phanerozoic tectonism in southwestern Montana basement ranges constrained by low temperature thermochronometric data: Tectonics, v. 40, https://doi.org/10.1029/2021TC006744.
- Karlstrom, K.E., and Timmons, J.M., 2012a, Many unconformities make one 'Great Unconformity,' in Timmons, J.M., and Karlstrom, K.E., eds., Grand Canyon Geology: Two Billion Years of Earth's History: Geological Society of America Special Paper 489, p. 73–79, https://doi.org/10.1130/2012.2489(04).
- Karlstrom, K.E., and Timmons, J.M., 2012b, Faulting and uplift in the Grand Canyon region, in Timmons, J.M., and Karlstrom, K.E., Grand Canyon Geology: Two Billion Years of Earth's History: Geological Society of America Special Paper 489, p. 93–107, https://doi.org/ /10.1130/2012.2489(06).
- Karlstrom, K.E., Åhäll, K.I., Harlan, S.S., Williams, M.L., McLelland, J., and Geissman, J.W., 2001, Long-lived (1.8–1.0 Ga) convergent orogen in southern Laurentia, its extensions to Australia and Baltica, and implications for refining Rodinia: Precambrian Research, v. 111, no. 1–4, p. 5–30, https://doi.org/10.1016 /S0301-9268(01)00154-1.
- Karlstrom, K.E., Ilg, B.R., Williams, M.L., Hawkins, D.P., Bowring, S.A., Seaman, S.J., Beus, S.S., and Morales, M., 2003, Paleoproterozoic rocks of the Granite Gorges: Grand Canyon Geology, v. 2, p. 9–38.
- Karlstrom, K.E., Lee, J.P., Kelley, S.A., Crow, R.S., Crossey, L.J., Young, R.A., Lazear, G., Beard, L.S., Ricketts, J.W., Fox, M., and Shuster, D.L., 2014, Formation of the Grand Canyon 5 to 6 million years ago through integration of older palaeocanyons: Nature Geoscience, v. 7, no. 3, p. 239–244, https://doi.org/10.1038 /ngeo2065.
- Karlstrom, K.E., Hagadorn, J., Gehrels, G.G., Mathews, W., Schmitz, M., Madronich, L., Mulder, J., Pecha, M., Geisler, D., and Crossey, L.J., 2018, Cambrian Sauk transgression in the Grand Canyon region redefined by detrital zircons: Nature Geoscience, v. 11, p. 438–443, https://doi.org/10.1038/s41561-018-0131-7.
- Karlstrom, K.E., Mohr, M.T., Schmitz, M.D., Sundberg, F.A., Rowland, S.M., Blakey, R., Foster, J.R., Crossey, L.J., Dehler, C.M., and Hagadorn, J.W., 2020, Redefining the Tonto Group of Grand Canyon and recalibrating the Cambrian time scale: Geology, v. 48, p. 425–430, https://doi.org/10.1130/G46755.1.
- Karlstrom, K.E., Crossey, L.J., Mathis, A., and Bowman, C., 2021, Telling time at Grand Canyon National Park:

- 2020 Update: Natural Resource Report NPS/GRCA/NRR-2021/2246.
- Karlstrom, K.E., Guenthner, W.R., Thurston, O.G., Heizler, M.T., Ricketts, J.W., and Timmons, J.M., 2022, COM-MENT Zircon (U-Th)/He thermochronology reveals pre-Great Unconformity paleotopography in the Grand Canyon region, USA: Geology, v. 50, e543, https://doi .org/10.1130/G49843C.1.
- Keller, C.B., Husson, J.M., Mitchell, R.N., Bottke, W.F., Gernon, T.M., Boehnke, P., Bell, E.A., Swanson-Hysell, N.L., and Peters, S.E., 2019, Neoproterozoic glacial origin of the Great Unconformity: Proceedings of the National Academy of Sciences of the United States of America, v. 116, p. 1136–1145, https://doi.org/10.1073/pnas.1804350116.
- Ketcham, R.A., 2005, Forward and inverse modeling of low-temperature thermochronometry data: Reviews in Mineralogy and Geochemistry, v. 58, p. 275–314, https://doi.org/10.2138/rmg.2005.58.11.
- Lee, J.P., Stockli, D.F., Kelley, S.A., Pederson, J.L., Karlstrom, K.E., and Ehlers, T.A., 2013, New thermochronometric constraints on the Tertiary landscape evolution of the central and eastern Grand Canyon, Arizona: Geosphere, v. 9, p. 216–228, https://doi.org/10.1130/GES00842.1.
- Lovera, O.M., 1992, Computer programs to model <sup>40</sup>Ar/<sup>39</sup>Ar diffusion data from multidomain samples: Computers & Geosciences, v. 18, p. 789–813, https://doi.org/10.1016/0098-3004(92)90025-M.
- Lovera, O.M., Richter, F.M., and Harrison, T.M., 1989, <sup>40</sup>Ar/<sup>39</sup>Ar thermochronometry for slowly cooled samples having a distribution of diffusion domain sizes: Journal of Geophysical Research: Solid Earth, v. 94, p. 17,917–17,935, https://doi.org/10.1029/JB094iB12p17917.
- Mahon, R.C., Dehler, C.M., Link, P.K., Karlstrom, K.E., and Gehrels, G.E., 2014, Geochronologic and stratigraphic constraints on the Mesoproterozoic and Neoproterozoic Pahrump Group, Death Valley, California: A record of the assembly, stability, and breakup of Rodinia: Geological Society of America Bulletin, v. 126, p. 652–664, https://doi.org/10.1130/B30956.1.
- McDannell, K.T., and Flowers, R.M., 2020, Vestiges of the ancient: Deep-time noble gas thermochronology: Elements, v. 16, p. 325–330, https://doi.org/10.2138/gselements.16.5.325.
- McDannell, K.T., and Keller, C.B., 2022, Cryogenian glacial erosion of the central Canadian Shield: The "late" Great Unconformity on thin ice: Geology, v. 50, p. 1336–1340, https://doi.org/10.1130/G50315.1.
- McDannell, K.T., Zeitler, P.K., and Schneider, D.A., 2018, Instability of the southern Canadian Shield during the late Proterozoic: Earth and Planetary Science Letters, v. 490, p. 100–109, https://doi.org/10.1016/j.epsl.2018 .03.012.
- McDannell, K.T., Schneider, D.A., Zeitler, P.K., O'Sullivan, P.B., and Issler, D.R., 2019, Reconstructing deep-time histories from integrated thermochronology: An example from southern Baffin Island, Canada: Terra Nova, v. 31, p. 189–204, https://doi.org/10.1111/ter.12386.
- McDannell, K.T., Keller, C.B., Guenthner, W.R., Zeitler, P.K., and Shuster, D.L., 2022a, Thermochronologic constraints on the origin of the Great Unconformity: Proceedings of the National Academy of Sciences of the United States of America, v. 119, https://doi.org/10 .1073/pnas.2118682119.
- McDannell, K.T., Pinet, N., and Issler, D.R., 2022b, Exhuming the Canadian Shield: Preliminary interpretations from low-temperature thermochronology and significance for the sedimentary succession of the Hudson Bay basin, in Lavoie, D., and Dewing, K., eds., Sedimentary Basins of Northern Canada: Contributions to a 1000 Ma Geological Journey and Insight on Resource Potential: Geological Survey of Canada Bulletin 609, p. 287–322, https://doi.org/10.4095/326100.
- McDannell, K.T., Keller, C.B., Guenthner, W.R., Zeitler, P.K., and Shuster, D.L., 2022c, Reply to Flowers et al.: Existing thermochronologic data constrain Snowball glacial erosion below the Great Unconformity: Proceedings of the National Academy of Sciences of the United States of America, v. 119, https://doi.org/10.1073/pnas.2209946119.

- McDermott, J., 2011, Microstructural, geochronologic and thermochronologic evidence for both Paleo- and Mesoproterozoic displacement across the Gneiss Canyon shear zone: Lower Granite Gorge, Grand Canyon, Arizona [M.S. thesis]: Albuquerque, New Mexico, University of New Mexico, 69 p.
- Mohr, M.T., Schmitz, M.D., Swansen-Hysell, N.L., Karlstrom, K.E., MacDonald, F.A., Holland, M., Zhang, Y., and Anderson, N., 2024, High-precision U-Pb geochronology links magmatism in the SW Laurentia Large Igneous Province and Midcontinent Rift: Geology, v. 52, p. 193–198, https://doi.org/10.1130/G51786.1.
- Mulder, J.A., Karlstrom, K.E., Fletcher, K., Heizler, M.T., Timmons, J.M., Crossey, L.J., Gehrels, G.E., and Pecha, M., 2017, The syn-orogenic sedimentary record of the Grenville Orogeny in southwest Laurentia: Precambrian Research, v. 294, p. 33–52, https://doi.org/10 .1016/j.precamres.2017.03.006.
- Nelson, L.L., Smith, E.F., Hodgin, E.B., Crowley, J.L., Schmitz, M.D., and MacDonald, F.A., 2020, Geochronological constraints on Neoproterozoic rifting and onset of the Marinoan glaciation from the Kingston Peak Formation in Death Valley, California (USA): Geology, v. 48, p. 1083–1087, https://doi.org/10.1130 //G47668.1.
- Peak, B.A., Flowers, R.M., Macdonald, F.A., and Cottle, J.M., 2021, Zircon (U-Th)/He thermochronology reveals pre-Great Unconformity paleotopography in the Grand Canyon region, USA: Geology, v. 49, p. 1462– 1466, https://doi.org/10.1130/G49116.1.
- Peak, B.A., Flowers, F.A., Macdonald, F.A., and Cottle, J.M., 2022, Zircon (U-Th)/He thermochronology reveals pre-Great Unconformity paleotopography in the Grand Canyon region, USA: REPLY: Geology, v. 50, e544, https://doi.org/10.1130/G49965Y.1.
- Peters, S.E., and Gaines, R.R., 2012, Formation of the 'Great Unconformity' as a trigger for the Cambrian explosion:

- Nature, v. 484, p. 363–366, https://doi.org/10.1038/nature10969.
- Porter, S.M., 2016, Tiny vampires in ancient seas: Evidence for predation via perforation in fossils from the 780– 740 million-year-old Chuar Group, Grand Canyon, USA: Proceedings: Biological Sciences, v. 283, https://doi.org/10.1098/rspb.2016.0221.
- Powell, J.W., 1875, Exploration of the Colorado River of the West and Its Tributaries: Smithsonian Institution Annual Report, 291 p.
- Powell, J.W., 1876, Report on the Geology of the Eastern Portion of the Uinta Mountains and a Region of Country Adjacent Thereto: U.S. Geological Survey Monograph, 218 p., https://doi.org/10.3133/70039913.
- Ricketts, J.W., Roiz, J., Karlstrom, K.E., Heizler, M.T., Guenthner, W.R., and Timmons, J.M., 2021, Tectonic controls on basement exhumation in the southern Rocky Mountains (United States): The power of combined zircon (U-Th)/He and K-feldspar <sup>40</sup>Ar/<sup>39</sup>Ar thermochronology: Geology, v. 49, p. 1187–1192, https://doi.org/10.1130/G49141.1.
- Robinson, K., 1994, Metamorphic petrology of the Lower Granite Gorge and the significance of the Gneiss Canyon shear zone: Grand Canyon, Arizona [M.S. thesis]: Amherst, Massachusetts, University of Massachusetts.
- Sanders, R.E., Heizler, M.T., and Goodwin, L.B., 2006, <sup>40</sup>Ar/<sup>39</sup>Ar thermochronology constraints on the timing of Proterozoic basement exhumation and fault ancestry, southern Sangre de Cristo Range, New Mexico: Geological Society of America Bulletin, v. 118, p. 1489– 1506, https://doi.org/10.1130/B25857.1.
- Sharp, R.P., 1940, Ep-Archean and Ep-Algonkian erosion surfaces, Grand Canyon, Arizona: Geological Society of America Bulletin, v. 51, p. 1235–1269, https://doi .org/10.1130/GSAB-51-1235.
- Thurston, O.G., Guenthner, W.R., Karlstrom, K.E., Ricketts, J.W., Heizler, M.T., and Timmons, J.R., 2022, Zircon (U-Th)/He thermochronology of Grand Canyon re-

- solves 1250 Ma unroofing at the Great Unconformity and <20 Ma canyon carving: Geology, v. 50, p. 222–226, https://doi.org/10.1130/G48699.1.
- Timmons, J.M., Karlstrom, K.E., Dehler, C.M., Geissman, J.W., and Heizler, M.T., 2001, Proterozoic multistage (~1.1 and ~0.8 Ga) extension in the Grand Canyon Supergroup and establishment of northwest and north-south tectonic grains in the southwestern United States: Geological Society of America Bulletin, v. 113, p. 163–180, https://doi.org/10.1130/0016-7606(2001)113-0163:PMCAGE>2.0.CO;2.
- Timmons, J.M., Karlstrom, K.E., Heizler, M., Bowring, S.A., and Crossey, L.C., 2005, Tectonic inferences from the ca. 1254–1100 Ma Unkar Group and Nankoweap Formation, Grand Canyon: Intracratonic deformation and basin formation during protracted Grenville orogenesis: Geological Society of America Bulletin, v. 117, p. 1573–1595, https://doi.org/10.1130 //B/5538 1
- Wang, R., Shen, B., Lang, X., Wen, B., Mitchell, R.N., Ma, H., Yin, Z., Peng, Y., Liu, Y., and Zhou, C., 2023, A Great late Ediacaran ice age: National Science Review, v. 10, https://doi.org/10.1093/nsr/nwad117.
- Yonkee, W.A., Dehler, C.D., Link, P.K., Balgord, E.A., Keeley, J.A., Hayes, D.S., Wells, M.L., Fanning, C.M., and Johnston, S.M., 2014, Tectono-stratigraphic framework of Neoproterozoic to Cambrian strata, west-central U.S.: Protracted rifting, glaciation, and evolution of the North American Cordilleran margin: Earth-Science Reviews, v. 136, p. 59–95, https://doi.org/10.1016/j.earscirev.2014 .05.004.

SCIENCE EDITOR: BRAD SINGER ASSOCIATE EDITOR: EMILY FINZEL

Manuscript Received 26 September 2023 Revised Manuscript Received 20 January 2024 Manuscript Accepted 25 March 2024